



Bachelor of Engineering  
(Mechanical)

PARAMETRIC GEOMETRICAL MODELLING OF  
WIND TURBINE BLADES & HUB

(Report on Capstone Project II)

By  
Aidar Kurmantayev  
Yerkegali Metey  
Saltanat Nazarova

Principal Supervisor: Konstantinos Kostas

April, 2017

## DECLARATION

We hereby declare that this report entitled “Parametric Geometrical Modelling Of Wind Turbine Blades & Hub” is the result of our own project work except for quotations and citations which have been duly acknowledged. We also declare that it has not been previously or concurrently submitted for any other degree at Nazarbayev University.

-----  
Name: Aidar Kurmantayev

Date: 21.04.17

-----  
Name: Yerkegali Metey

Date: 21.04.17

-----  
Name: Saltanat Nazarova

Date: 21.04.17

## **ABSTRACT**

Wind turbine industry has substantially grown in last decades and is still becoming larger. Hence, effective ways to design wind turbines are needed. In this report, the procedure of parametric design of a wind turbine blade is presented. This is performed with the help of Grasshopper®, an application embedded into Rhinoceros 3D graphical design software. The process involves parametric construction of airfoil sections along the wind turbine blade. The geometry is modeled by taking advantage of Bezier curves, since they can be used to build nonlinear high curvature contours. Main feature curves in an airfoil are the camber, upper and lower sides, which are defined by a set of appropriately selected parameters. The generation of multiple airfoil sections enables us to construct a complete 3D shape with help of the lofting feature in Rhinoceros environment. Results can be further utilized for static or dynamic analysis. The aim of the project is to develop an algorithm that enables us to reconstruct any available wind turbine blade with maximum precision and to establish a verified solution method by reproducing published data for NACA 4412 in the subsonic flow regime. The blade design is described in detail in this report and all the stages are presented with appropriate illustrations.

## TABLE OF CONTENTS

1. INTRODUCTION.....	1
1.1. Problem Statement.....	1-2
1.2. Project Description.....	2-3
1.3. Practical Application.....	3-4
1.4. Airfoil.....	4-7
1.5. Bezier Curve.....	7-8
2. LITERATURE REVIEW.....	9
2.1. Design and Analysis of A Vertical Axis Wind Turbine Blade Using Analytical And Numerical Techniques .....	9-11
2.2. Computer-Aided Design of Horizontal Axis Turbine Blades.....	11-12
2.3. Optimization Design, Modeling and Dynamic Analysis for Composite Wind Turbine Blade.....	12-14
2.4. T4T (Tools for Turbomachinery) software .....	14-16
3. METHODOLOGY.....	16
3.1. Construction of The Model.....	16-18
3.1.1. Camber Curve.....	18-21
3.1.2. Upper Curve.....	21-23
3.1.3. Lower Curve.....	23-24
3.1.4. Airfoil Algorithm.....	24-25
3.1.5. Read File Component.....	25
3.2. Blade Surface Definition.....	25-26
3.3. Geometry Description.....	26-27
4. ANSYS FLUENT SIMULATION.....	27
4.1. Description of Tool.....	27-28
4.2. Inputs and Constraints.....	28
4.3. Simulation Procedure.....	28-29
4.3.1. Turbulence Model.....	29-30
4.3.2. Geometry.....	30-31
4.3.3. Mesh Control.....	31-34
4.3.4. Set Up Procedure.....	35-39
5. OPTIMIZATION EXAMPLE.....	39
6. RESULTS.....	40-41
7. CONCLUSION AND DISCUSSION.....	41-42
REFERENCE LIST.....	2
APPENDICES.....	A-P

## LIST OF FIGURES

- Figure 1.1.1: World Energy Consumption 2000-2015 years  
Figure 1.1.2: Alternative configurations for shaft and rotor orientation  
Figure 1.4.1: Airfoil  
Figure 1.5.1: Examples of Bezier Curves  
Figure 1.5.2: Bezier curves of various degrees  
Figure 2.1.1: Maximum deflection graph  
Figure 2.1.2: Maximum stress graph  
Figure 2.3.1: Cross-section charts of blade elements  
Figure 2.4.1: Mean camber line and inscribed circles between pressure and suction sides  
Figure 2.4.2: 3D blade along with its cross sections  
Figure 3.1.1.1: Airfoil parameters  
Figure 3.1.1.2: Construction algorithm of camber curve in Grasshopper software  
Figure 3.1.1.3: Camber curve in Rhinoceros software  
Figure 3.1.2.1: Construction algorithm of upper curve in Grasshopper software  
Figure 3.1.2.2: Upper curve in Rhinoceros software  
Figure 3.1.3.1: Construction algorithm of lower curve in Grasshopper software  
Figure 3.1.3.2: Lower curve in Rhinoceros software  
Figure 3.1.4.1: Airfoil algorithm  
Figure 4.1.1: Blade construction in 3D space  
Figure 4.2.2: S809 Airfoil points and produced airfoil  
Figure 4.2.1: S809 Airfoil shape  
Figure 4.3.1: Whole procedure in ANSYS Workbench  
Figure 4.3.2.1: Geometry of a wind tunnel and airfoil at an angle of  $0^\circ$   
Figure 4.3.3.1: Wind tunnel at an angle of  $0^\circ$   
Figure 4.3.3.2: Mesh of a wind tunnel at an angle of  $0^\circ$   
Figure 4.3.3.3: Scaled mesh of an airfoil at an angle of  $0^\circ$   
Figure 4.3.3.4: Inflation of an airfoil mesh at an angle of  $0^\circ$   
Figure 4.3.3.5: Edge sizing of an airfoil edges at an angle of  $0^\circ$   
Figure 5.1: Shape of optimized airfoil  
Figure 7.1:  $C_L$  coefficient data from airfoiltools.com  
Figure 7.2:  $C_D$  coefficient data from airfoiltools.com  
Figure 1. Scaled mesh of an airfoil at an angle of  $1^\circ$   
Figure 2. Scaled mesh of an airfoil at an angle of  $3^\circ$   
Figure 3. Inflation of an airfoil mesh at an angle of  $1^\circ$   
Figure 4. Inflation of an airfoil mesh at an angle of  $3^\circ$   
Figure 5. Inflation of an airfoil mesh at an angle of  $5^\circ$

## LIST OF TABLES

- Table 2.1.1: Parameters for modeling*  
*Table 3.1.1: Components used in Grasshopper software*  
*Table 3.1.1.1: Parameters of camber curve and its abbreviations*  
*Table 3.1.2.1: Parameters of upper curve and its abbreviations*  
*Table 5.1: Inviscid solver and ANSYS Fluent results*  
*Table 6.1: Results of ANSYS FLUENT simulation*  
*Table 7.1: Data taken from airfoiltool.com*  
*Table 1. S809 Airfoil Coordinates*  
*Table 2. Model Orifice Locations*  
*Table 2. Model Orifice Locations (Concluded)*  
*Table 3. Airfoil Design Specifications (S809)*  
*Table 4. Roughness Size and Location*  
*Table 5. AOA1 > Geometry*  
*Table 6. AOA1 > Geometry > Parts*  
*Table 7. AOA1 > Connections*  
*Table 8. AOA1 > Mesh*  
*Table 9. AOA1 > Mesh > Mesh Controls*  
*Table 10. AOA3 > Geometry*  
*Table 11. AOA3 > Geometry > Parts*  
*Table 12. AOA3 > Connections*  
*Table 13. AOA3 > Mesh*  
*Table 14. AOA3 > Mesh > Mesh Controls*  
*Table 15. AOA5 > Geometry*  
*Table 16. AOA5 > Geometry > Parts*  
*Table 17. AOA5 > Connections*  
*Table 18. AOA5 > Mesh*  
*Table 19. AOA5 > Mesh > Mesh Controls*

## LIST OF ABBREVIATIONS, NOTATIONS / GLOSSARY OF TERMS

Measurements and calculations were made in SI Units.

$C_p$	pressure coefficient
$c$	airfoil chord
$c_d$	section profile-drag coefficient
$c_l$	section lift coefficient
$c_m$	section pitching-moment coefficient about quarter-chord point
L.	lower surface
M	Mach number
max	maximum (subscript)
NREL	National Renewable Energy Laboratory
R	Reynolds number based on free-stream conditions and airfoil chord
S.	boundary-layer separation location, $1 - s_{sep}/c$
$s_{sep}$	arc length along which boundary layer is separated
$s_{turb}$	arc length along which boundary layer is turbulent including $s_{sep}$
T	transition (subscript)
T.	boundary-layer transition location, $1 - s_{turb}/c$
U.	upper surface
x	airfoil abscissa
y	model span station, $y = 0$ at midspan, positive downward
z	airfoil ordinate
$\alpha$	angle of attack relative to x-axis
HAWT	horizontal axis wind turbine
VAWT	vertical axis wind turbine



# 1. INTRODUCTION

## 1.1. Problem Statement

The energy consumption over the world has been constantly growing over the decades from just under 10 000 million tonnes of oil equivalent in 2000 to almost 13,500 in year 2015 as illustrated in Figure 1.1.1[2]. Conventional energy sources have been shown to have detrimental effect on the environment. The exploitation of sustainable energy sources appears to be one of the most feasible solutions to this problem.

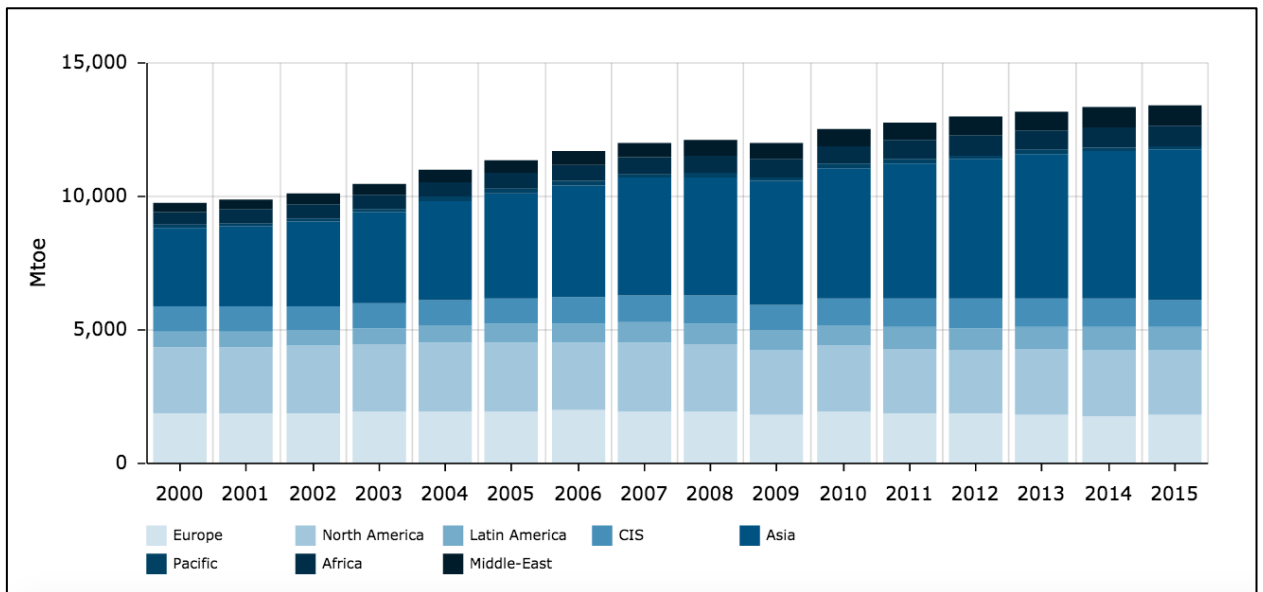
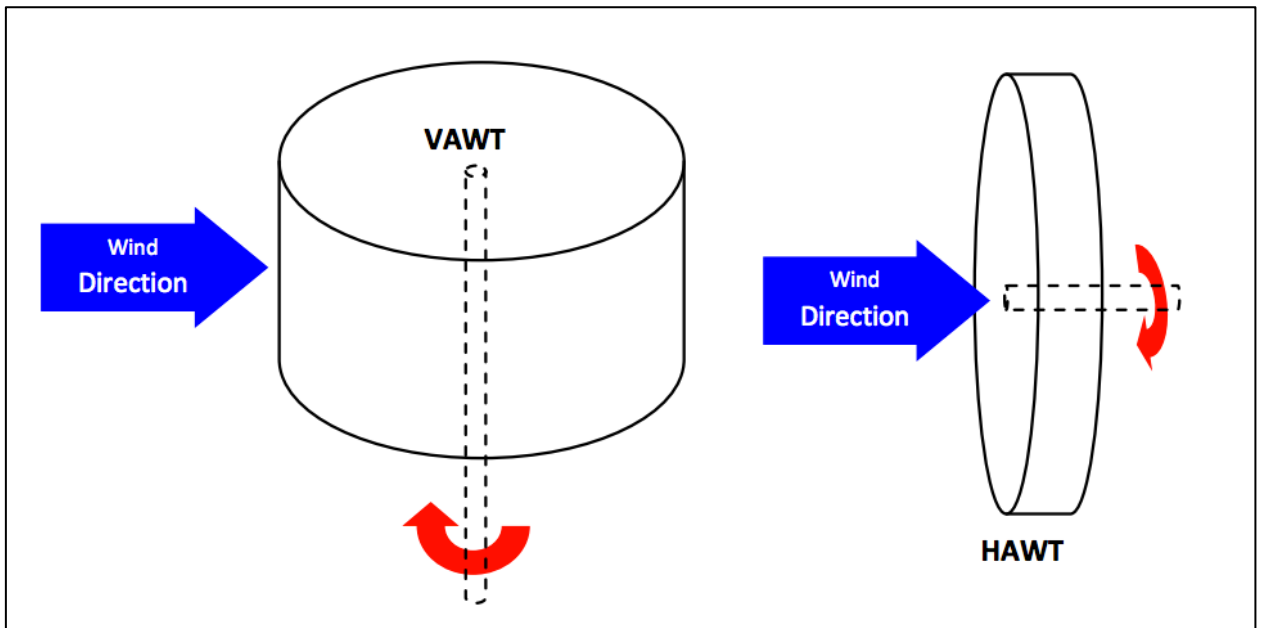


Figure 1.1.1: World Energy Consumption 2000-2015year

Indeed, wind is an abundant, free and clean source of energy. Thus, wind turbines have become one of the most popular tools in sustainable energy exploitation. Wind turbines can be classified as horizontal axis HAWT and vertical axis wind turbines VAWT depending on the orientation of their shaft and rotational axis as shown in Figure 1.1.2 [6]. Currently, HAWT turbines are more widely used comparing to VAWT. Thus, wind turbines are differentiated based on their design. Overall, a typical wind turbine's design whether it is HAWT or VAWT consists of blades, hub and tower.



*Figure 1.1.2: Alternative configurations for shaft and rotor orientation*

Wind turbines are consistently undergoing design alterations to improve their efficiency and reduce cost. The design of blades has an essential role in the development of the wind turbines, as the blades are the part of the wind turbine that capture the wind and generate the energy [3]. It is a scrupulous work that requires tremendous efforts and time. The aim of the project is to contribute to facilitation of this process by developing the methodology and the software tools that allow the automatic generation of 3D surface and mesh models of wind turbine blades and the accompanying hub. The project consists of two parts. The first part delivered this semester focuses on the development of the methodology and design of the blades, while the second part concentrates on the design of the hub and optimization of the results.

## **1.2. Project Description**

In order to automatically generate 3D surfaces of the blades, the number of their cross-sections that is airfoils are considered. Each airfoil based on its geometrical parameters is constructed in Grasshopper software. Geometrical parameters are chosen as the minimum number of parameters that permits the user to create a wide variety of shape instances offering at the same time the maximum flexibility. The only problem

that was encountered during this project was transferring the algorithm of the curve construction into Grasshopper building blocks, as this software is newly discovered for all the group members.

The main steps of the project are:

- ❖ Identification of the parameters that will be used in the generation wind turbine blades (number of blades, chord lengths, angles, radii etc / length, camber width, trailing edge angle etc)
- ❖ Generation of a curve grid comprising basic and auxiliary guiding curves that are appropriate for the shape description of the wind turbine
- ❖ Generation of modeling aids (auxiliary curves and/or surfaces), if required
- ❖ Generation of the 3d surface model of blades by interpolation of control curve grid
- ❖ Modeling of the existing airfoil shapes
- ❖ ANSYS Fluent simulation
- ❖ Optimization

The project is accomplished by a group consisting of three mechanical engineering students: Yerkegali Metey, Saltanat Nazarova and Aidar Kurmantayev. The main duties of each group member are:

- ❖ Literature review, data analysis and report editing - Saltanat Nazarova
- ❖ Generation of curves, ANSYS Fluent simulation, optimization - Yerkegali Matey and Aidar Kurmantayev
- ❖ Identification of parameters – team work.

### **1.3. Practical Application**

This project is vital to any user who is involved in wind turbine development. The deliverable of the project is a user-friendly tool based on Grasshopper software that

allow designing wind turbine blades based on the geometrical parameters. Hence, any user even from non-engineering field who has parametrical data can obtain the resultant blade once they input their data. Moreover, this tool may be exploited for modeling of existing airfoil shapes. Indeed, this tool is able to design the shape of a specific existing airfoil, thus the geometrical parameters of a specific shape can be obtained. Overall, this project may be used for research purposes, in wind turbine manufacturing field and by the students for educational purposes.

#### **1.4. Airfoil**

The lift force is generated due to the shape of the airfoil. It acts perpendicular to the direction of flow and is the net result of the pressure difference. Indeed, low air pressures act on the surface of the airfoil with more curve, while high-pressure air pushes on it's the other side. The lift force increases, as the blade is located at a greater angle to the wind that is angle of attack. At very large angles of attack the blade "stalls" and the lift decreases again. So there is an optimum angle of attack to generate the maximum lift.

Another force that acts on the airfoil is the drag force. It is parallel to the flow and increases with angle of attack. At an angle slightly less than the maximum lift angle, the blade reaches its maximum lift/drag ratio. The best operating point will be between these two angles [5].

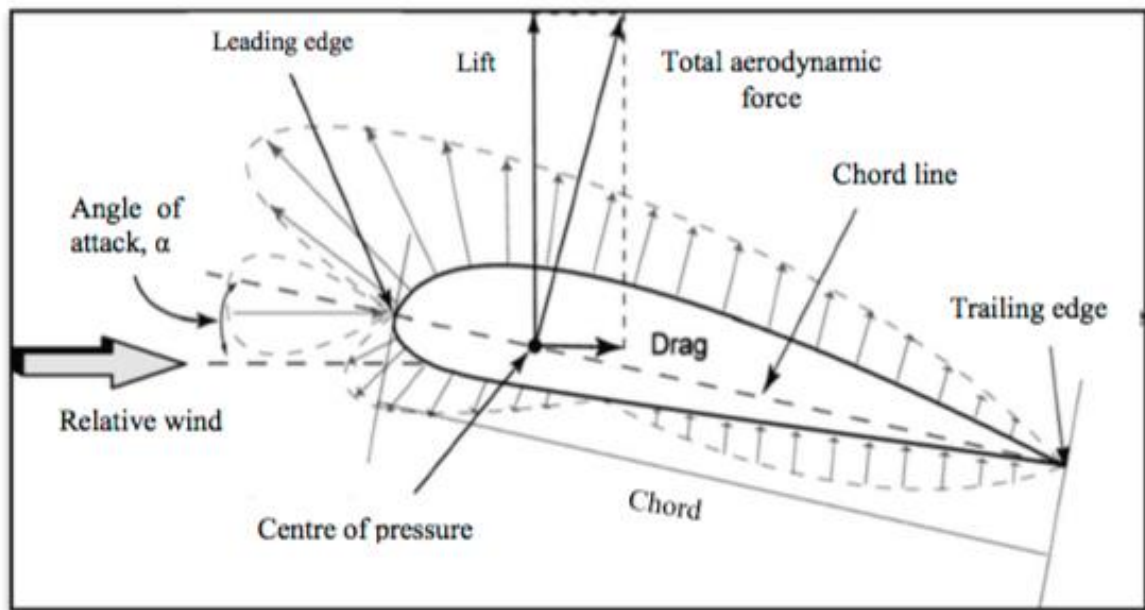


Figure 1.4.1: Airfoil

Since the drag is in the downwind direction, it may seem that it wouldn't matter for a wind turbine as the drag would be parallel to the turbine axis, so wouldn't slow the rotor down. It would just create "thrust", the force that acts parallel to the turbine axis hence has no tendency to speed up or slow down the rotor. When the rotor is stationary (e.g. just before start-up), this is indeed the case. However, the blade's own movement through the air means that, as far as the blade is concerned, the wind is blowing from a different angle. This is called apparent wind. The apparent wind is stronger than the true wind but its angle is less favourable. At this angle drag is increased, while the lifting force acting on the airfoil decreases. Thus, to maintain a good angle of attack, the blade must be turned further from the true wind angle.

Aerodynamics is a science that mainly focuses on the air movement around a solid body. This discipline has been born with the first attempts of humanity to construct airplanes. The theory behind aerodynamics is based on fluid and gas dynamics. Thus, it is a sub category of these disciplines with the difference that it is concerned mainly with air motion. Although formal development of this discipline began in the eighteenth century, the basic concepts, such as aerodynamic drag, had already been observed and understood earlier. One of the earliest experiments in aerodynamics has

aimed to achieve heavier-than-air flying machines, and was first illustrated in 1903 by Wilbur and Orville Wright. Since then, the science of aerodynamics has been constantly developing with the use of mathematical analysis and scientific experimentation in wind tunnels as well as computer based simulations. Currently it is focused on the study of more sophisticated concepts such as compressible flow, supersonic and subsonic flow, turbulence, boundary layers and has become increasingly computational in nature.

An airfoil is the cross-sectional shape of the wing. It is a fundamental unit in aerodynamics, as its study clearly demonstrates basic concepts of this science and simulations of the full number of the cross-sections of the wing provide comprehensive data for practical use. The typical shape of the airfoil is illustrated in Figure 1.4.1. As it is clearly shown, this shape is dependent on its chord line, chamber line, leading and trailing edge etc. These terms will be explained later.

An airfoil-shaped body, moving through a fluid, produces an aerodynamic force. The component of this force, perpendicular to the direction of motion, is called lift. The component parallel to the direction of motion is called drag.

The lift of an airfoil is mainly the result of its angle of attack and shape. When oriented at a suitable angle, the airfoil deflects the oncoming air, resulting in a force on the airfoil in the direction opposite to the deflection. This force is known as aerodynamic force and can be resolved into two components: lift and drag. Most foil shapes require a positive angle of attack to generate lift, but cambered airfoils can generate lift at zero angle of attack. This "turning" of the air near the airfoil creates curved streamlines, resulting in lower pressure on one side and higher pressure on the other. This pressure difference is accompanied by a velocity difference, as described by Bernoulli's principle, so the resulting flowfield about the airfoil has a higher average velocity on the upper surface than on the lower surface.

Terms related to the geometry of an airfoil:

- ❖ The *leading edge* is the foremost point of the airfoil. For a zero angle of attack, it coincides with the stagnation point.
- ❖ The *trailing edge* is the point at the end of the airfoil where the flow rejoins.
- ❖ The *chord line* is the straight line connecting leading and trailing edges.
- ❖ Angle of attack is the angle between the chord line and the direction of the oncoming flow.
- ❖ Camber line is the locus of points midway between the upper and lower surfaces. It may or may not be a straight line.
- ❖ Lift coefficient is a dimensionless coefficient that relates the lift force on the body to a reference area and to fluid's velocity and density.
- ❖ Drag coefficient is a dimensionless coefficient that relates the dragging force on the body to a reference area and to fluid's velocity and density.
- ❖ Stall angle of attack is the angle of attack at which the lift coefficient is maximum and after which the lift coefficient starts to decrease.

## 1.5. Bezier Curve

The algorithm of construction of airfoils in Grasshopper is based on Bezier curves. It is the curves that are developed with the use of control polygons that are comprised of control points. Figure 1.5.1 shows the examples of Bezier curves. Bezier curve passes through its first and last control points, and is tangent to the control polygon at those endpoints. Complicated shapes can be designed by using a number of Bezier curves. Since Bezier curves are tangent to their control polygons, it is easy to join together two Bezier curves such that they are tangent continuous. Bezier curves of any degree can be defined. Figure 1.5.2 shows Bezier curves of various degrees [7]. A degree  $n$  Bezier curve has  $n + 1$  control points. In this project degree  $n=2$  and  $n=3$  are used. A mathematical equation that is used for Bezier curve construction has a form of:

$$P(t) = m_0(t)P_0 + m_1(t)P_1 + m_2(t)P_2 + m_3(t)P_3. \quad [1.5.1]$$

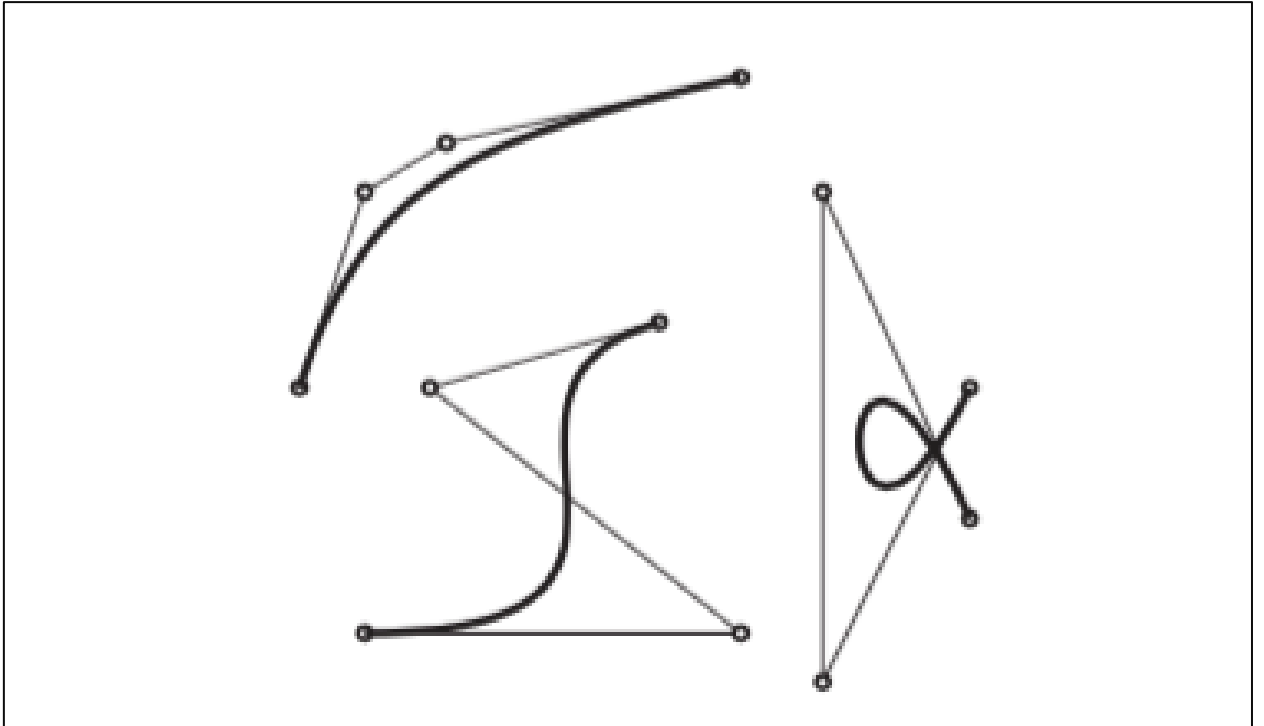


Figure 1.5.1: Examples of Bezier Curves

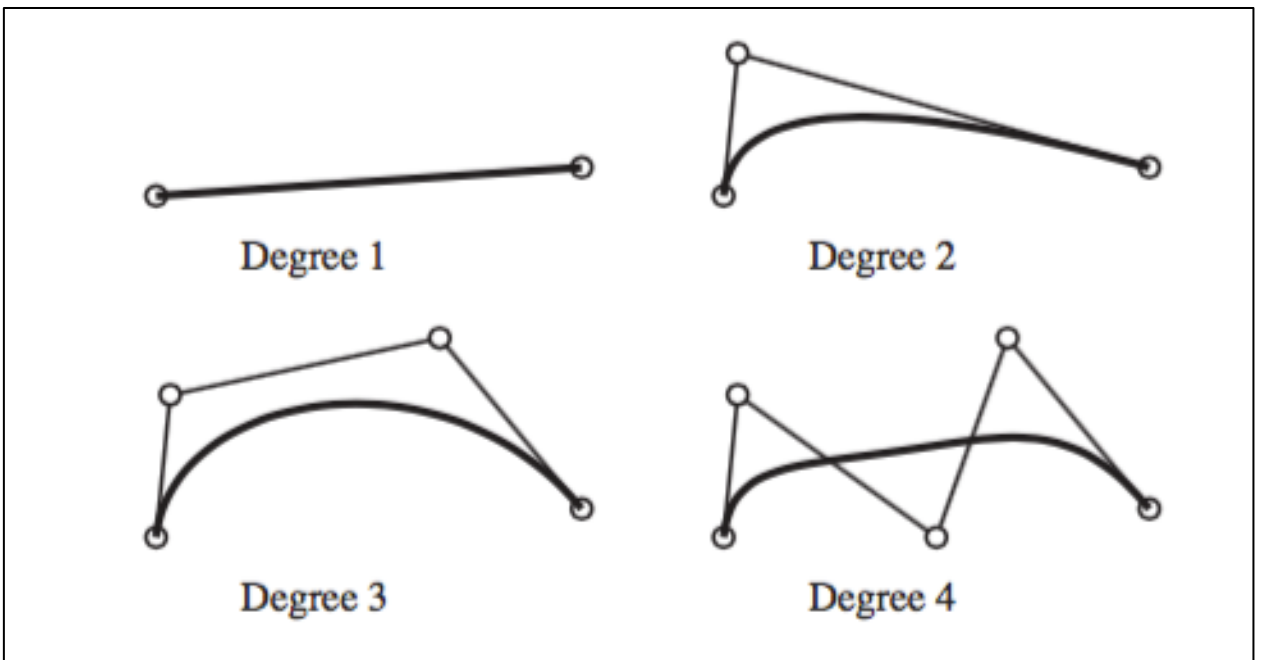


Figure 1.5.2: Bezier curves of various degrees

## **2. LITERATURE REVIEW**

Various methods are currently being developed in the field of detailed wind turbine modeling. Different views and approaches on how to design each crucial shape are employed, such as taking advantage of B-spline curves and inserting parameters for such curves or constructing outer shape by generating points on a 2D plane etc. are implemented to achieve that objective. In following literature review some of these methods will be presented.

### **2.1. Design And Analysis Of A Bladed Vertical Axis Wind Turbine Blade Using Analytical And Numerical Techniques**

Hameed and Afaq [4] focused on design and optimization of the Vertical Axis Wind Turbine (VAWT) using analytical and numerical techniques. This type of turbine has the advantage of allowing separate placement of the wind capturing component and the generator, which can be installed on the ground. In addition, VAWT is able to handle wind coming from any direction without yawing. The blades are straight, untwisted and uniform sectioned, therefore are easy to fabricate. However, though the benefits of this turbine are motivating, there are still risks involved. Comparing to the width of a blade, its length is very big, hence the aspect ratio is substantially large and when high values of bending moments appear in its weakest points, the result can be a failure of that blade. The solution proposed was a three-blade design, which will alleviate the stresses at the connection between the blade and a tower. The blade model specifications were calculated analytically, the model was justified numerically and the optimum value of the wall thickness was determined for highest values of bending stresses and deflections.

There is a substantial number of design parameters incorporated in this research. Following is the table describing each of them.

Table 2.1.1: Parameters for Modeling

Design velocity, $V$	The average operational wind speed was taken as 8 m/s
No. of blades, $n$	Three or more blades can reduce the torque ripple
Tip speed ratio, TSR	Ratio between rotational speed of the blade tip and wind velocity
Solidity	The ratio of blade area and rotor area
Power coefficient, $C_p$	For TSR=4.1, solidity=0.24, $C_p=0.43$
Diameter of turbine, $D$	For 900 W output and density of air as 1.23 Kg/m <sup>3</sup> , $D=2.578\text{m}$
Span length of the blade, $b$	Span was also taken as 2.578m
Aspect ratio, AR	For straight bladed VAWT, AR=12.5
Chord length of the blade, $c$	Calculated value for chord length was 0.2062m
Selection of airfoil	NACA 0015 was chosen as most suitable because of desired aerodynamic performance

First thing the researchers did was finding the relation between angle of attack and a pitching angle. The various values of angles and their relations were tabulated and plotted versus each other. After that lift and drag coefficients were calculated utilizing commercial DESFOL software. They were also inserted in a table sorting them accordingly to a pitch angle. Next was evaluating maximum tangential blade velocity  $R_w$ , which was equal to 32.8 m/s. Relative velocity as a vector solution of maximum blade tip velocity and velocity  $V$  was calculated for various angles inside velocity triangle. Normal and axial forces were determined in complete rotation of a blade. Then locations of strut attachment with the blade and cross sectional parameters were identified. The design material was selected to be aluminum with  $E=70\text{ GPa}$ ,  $\rho=2700\text{ Kg/m}^3$  and  $\nu=0.33$ . After calculating the centrifugal forces, finally, maximum deflections and stresses were evaluated and recorded.

Numerical evaluations involved subjecting the model under the same boundary conditions, and altering the wall thicknesses and element type specifications in ANSYS 11.0 library. The difference between numerical and analytical models is represented in following pictures. Solid45 and Beam3 are element types chosen from ANSYS library in order to compare the convergence of solutions to analytical ones.

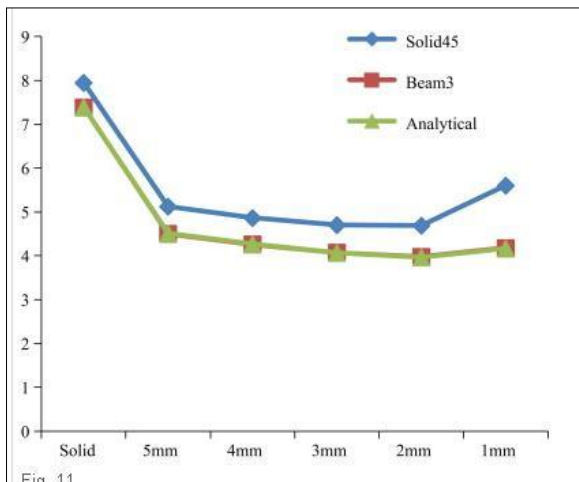


Figure 2.1.1: Maximum deflection graph

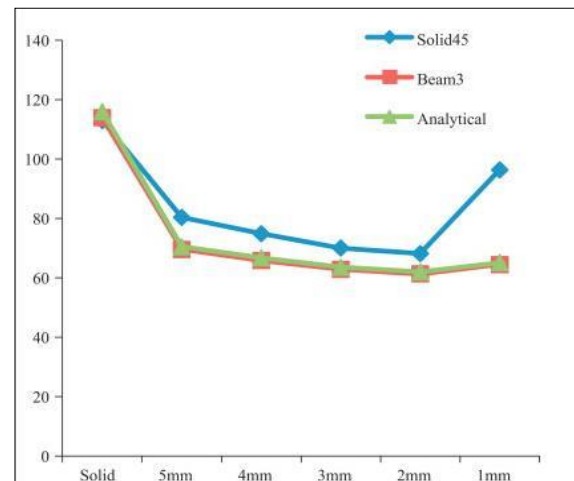


Figure 2.1.2: Maximum stress graph

Figures indicate after specifying the element type to Beam3, the analytical and numerical solutions become similar. This purpose of this part of literature review was to illustrate one type of wind turbine blade modeling. The geometry was optimized firstly basing on the beam theory, and after that it was numerically modeled.

## 2.2. Computer-Aided Design Of Horizontal Axis Turbine Blades

Next research employs a distinct approach in designing a wind turbine blade. Specifically, Perez and Vargas present a method that utilizes B-spline surfaces realized in computer environment [6]. They have done their work in QBLADE, the platform for wind turbine blade design and aerodynamic simulation [11]. A horizontal axis rotor is made of several twisted blades uniformly placed around a hub. A series of airfoil sections define the surface of those blades, alternating from a circular shape near the hub up to sharp streamlined surfaces at the tip of the blade. The 3D model of blade is constructed via interpolation between multiple curves in 3D space, which are indeed cross sections of a blade. In order to build these curves it is required to accurately represent the shape of an airfoil in the software. Standard approaches require working with large amount of data in turn, because more than hundred discrete points are needed to capture airfoil shape. The reason behind this is the leading edge of the airfoil,

which has high curvature, compared to its rear part, and this leading edge possesses most aerodynamic properties of the turbine.

The method comprises the following: the geometric parameters of the blade are recorded firstly, being the position, skew, rake, and twist distribution and the sectors, which were defined discretely. Next, curve-fitting scheme is implemented and B-spline curves emerge as a result. Finally, a lofting procedure is applied and the 3D exterior surface is generated. The crucial point here is that all mentioned parameters help to define coordinates of a curve relative to an origin. The derived equation is following

$$Q_j = (r_i \cdot \sin(\alpha_i + Sk_i), R \cdot \sin(\theta + Tw_i) + Rk_i, r_i \cdot \cos(\alpha_i + Sk_i)) \quad [2.2.1]$$

Where  $r_i$  is the coordinate vector radius

$Tw$  - twist angle

$Sk_i$  - skew angle

$Rk_i$  - rake angle

Several points are obtained, and a least squares approximation method is applied, so that the number of control points is not large. An iterative process is employed for acquiring the required shape accuracy for the resulting description.

Finally, the lofting process is curve interpolation process where the solution to systems of parameterized equations will provide the shape of the airfoil.

### **2.3. Optimization Design, Modeling and Dynamic Analysis for Composite Wind Turbine Blade**

Song et al claim that it is difficult to evaluate the most important features of wind turbine blades such as axial and circumferential factors [9]. The shape of blade is complex, and moreover, the materials of which modern turbine blades are made of (fiber glass and other composites) require accurate and precise modeling of their shape. The purpose of their research was to develop software that enables to aerodynamically

optimize and precisely reconstruct the blade in CAD program for further static and dynamical analysis.

The optimization process started from specifying standard parameters such as choosing the existing turbine model, its rotor diameter, and angle of attack at the blade, aiming to obtain to maximum wind energy utilization coefficient. It was based on Blade Element - Momentum Theory, and adopted for optimization by Wilson method [9]. The optimization algorithm was coded in MATLAB designed to obtain chord length and twist angle as utilization coefficient variables. The iterative loop was used and identified the most suitable needed values.

The geometrical blade modeling was performed by means of coordinate transformation. Taking the trailing edge as origin, the two and three-dimensional translation was applied. The example of such an equation is presented below

$$\begin{aligned} &\text{When } X < 0, \\ &\left\{ \begin{array}{l} X = -\frac{C}{100} \times \sqrt{X_1^2 + Y_1^2} \times \cos(\arctan \frac{Y_1}{X_1} + \theta) \\ Y = -\frac{C}{100} \times \sqrt{X_1^2 + Y_1^2} \times \sin(\arctan \frac{Y_1}{X_1} + \theta) \\ Z = r \end{array} \right. \end{aligned} \quad [2.3.1]$$

The coordinates were inserted and cross section profiles defined by set of dots were obtained. Following pictures illustrate charts resulting from transformation.

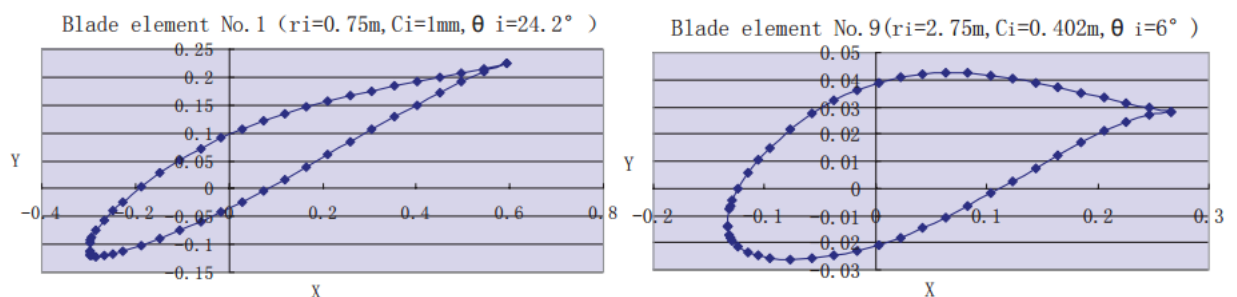


Figure 2.3.1: Cross-section charts of blade elements

To sum up, the authors applied MATLAB programming to shape the contour of wind turbine blades. Integrating data in SolidWorks and ANSYS allowed constructing 3D models to observe what the actual blade would look like.

#### **2.4. T4T (Tools for Turbomachinery) software.**

Strofylos et al. (2014) have developed a tool named “T4T” (Tools for Turbomachinery) for the parametric design of turbomachinery and wind turbine blades. The authors claim that precise and efficient geometry representation is a crucial point in either construction of new airfoils or in optimizing existing models. They developed a program in QT C++ which has some specific features such as the methodology to calculate the mean camber line, leading edge, chord for any arbitrary blade section, or ability to modify trailing edge and add thickness to it and others.

Two ways of constructing the blade profile are reported in their work. In the first the design procedure starts with a definition of the mean camber line, after which “thicknesses” are distributed along the airfoil and the profile is created. The second method involves importing points provided in a text file and fitting a curve higher than second degree to ensure continuity of 2<sup>nd</sup> derivatives. After outer curve is constructed, the mean camber line, leading edge and chord line computations are performed. However, to construct the mean camber line, a slightly complex procedure is carried out, because leading edge is usually unknown. The bisector line between upper and lower sides is approximated with help of circles inscribed in the profile. The centers of each circle are connected to form a curve and finally, the curve is extended along its tangent vector and its intersection with the profile curve defines the leading edge.

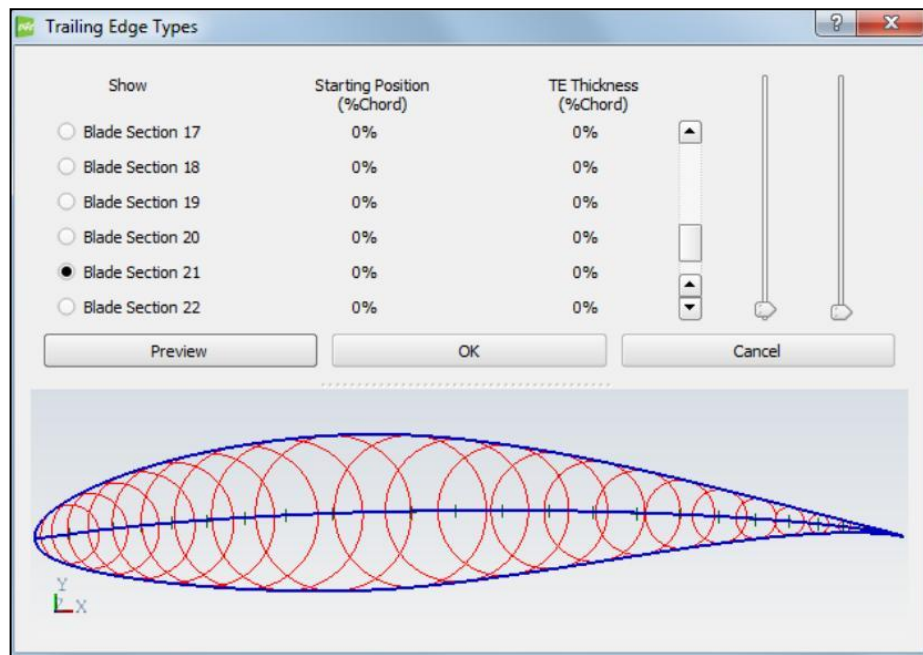


Figure 2.4.1: Mean camber line and inscribed circles between pressure and suction sides

To produce the 3D model, the blade profiles are distributed perpendicularly to the stacking line which is usually a straight line. They can be oriented with respect to their center of gravity or the leading edge, or some specific points such as aerodynamic center. After that the profiles are distributed in following manner.

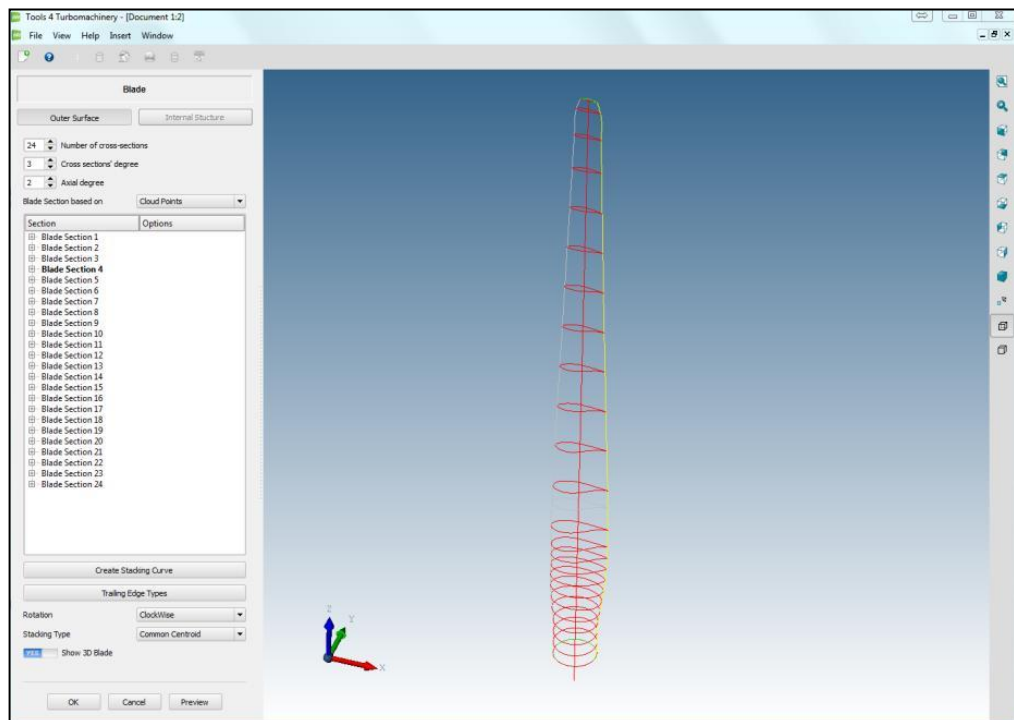


Figure 2.4.2: 3D blade along with its cross sections

Final step of outer 3D surface construction is the interpolation along the span of the turbine blade. The important note is that all profiles must have same number of interpolation points. The necessary points are computed using a cosine distribution and interpolation is performed. Strofylas et al. (2014) claim that this methodology ensures continuity of the surface, while some commercial software fail to carry out proper lofting procedure leaving inaccurate trailing and edge geometries.

Another research presented by Charalampous et al. (2015) demonstrates the methodology for the parametric design of wind turbine blades in Grasshopper 3D. The methodology is similar to what is done in our capstone except for the profile is again constructed from set of points fitted to a curve like mentioned above. The motivation behind is in the freedom provided by the Grasshopper 3D and Rhinoceros 3D in constructing various types of curves and shapes, while most of commercial software are limited in the complex shape definitions which in turn make it difficult to finalize the model. Authors claim that Grasshopper 3D not only overcomes the problem, but also enables them to construct parametric models for the geometric design specifications of wind turbine blades.

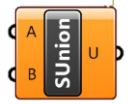
### **3. METHODOLOGY**

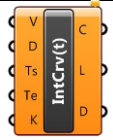
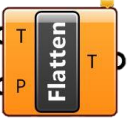
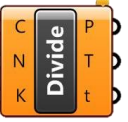
#### **3.1. Construction of The Model**

The blade is designed in Rhinoceros-3D with the aid of the Grasshopper® visual programming software package. This software was chosen as it has user-friendly interface. Eight parameters are employed for the design of an airfoil: camber curve parameters are angle at leading edge, angle at trailing angle, maximum camber width Y, and longitudinal position of maximum camber width X; upper side curve parameters are angle at trailing edge, maximum width Y, longitudinal position of maximum width X, and shape fullness at leading edge. An airfoil consists of upper, camber and lower curves. First, the camber curve is set up, then it is followed by upper curve the construction definition of which will be presented afterwards, and finally lower curve is constructed by mirroring selected points from upper curve about the camber curve and joining them in order to get lines between points. Consequently, these lines are mirrored about camber curve. End points of each line are interpolated to get lower

curve. Bezier curves are used to model curves. Especially, second and third-degree Bezier curves were utilized.

Table 3.1.1: Components used in Grasshopper® software

Components	Description
	<i>Point</i> - contains a collection of three-dimensional points
	<i>Number slider</i> - numeric slider for single values
	<i>Read File</i> - read the contents of a file
	<i>Remap Numbers</i> - remap numbers into a new numeric domain
	<i>Set Union</i> - creates the union of two sets (the collection of unique objects present in either set)
	<i>Nurbs Curve</i> - construct a nurbs curve from control points
	<i>Move</i> - translate (move) an object along a vector
	<i>Mirror Curve</i> - mirror a shape in a freedom curve
	<i>Loft</i> - create a lofted surface through a set of section curves
	<i>Line</i> - create a line between two points
	<i>Join Curves</i> - join as many curves as possible

	<p><i>Interpolate (t)</i> - create an interpolated curve through a set of points with tangents</p>
	<p><i>Flatten Tree</i> - flatten a data tree by removing all branching information</p>
	<p><i>Expression</i> - evaluate an expression</p>
	<p><i>End Points</i> - extract the end points of a curve</p>
	<p><i>Domain</i> - numeric domain between {A} and {B}</p>
	<p><i>Divide Curve</i> - divide a curve into equal length segments</p>
	<p><i>Curve Closest Point</i> - find the closest point on a curve</p>
	<p><i>Construct Point</i> - construct a point from {xyz} coordinates</p>

### 3.1.1. Camber Curve

The starting and end points of the curve are fixed and shown in the program as point 1 and point 5 in Grasshopper® model of camber curve. Their coordinates are (0,0) and (1,0) respectively. However, the length of the airfoil is set to (1,0) by default, so it can be set to any number and hence the last point could be noted as (L,0). Four parameters are allowed to be changed with the help of *Number Slider* component: leading edge angle, trailing edge angle and the coordinates of the max width of the curve, which are x\_max and y\_max.

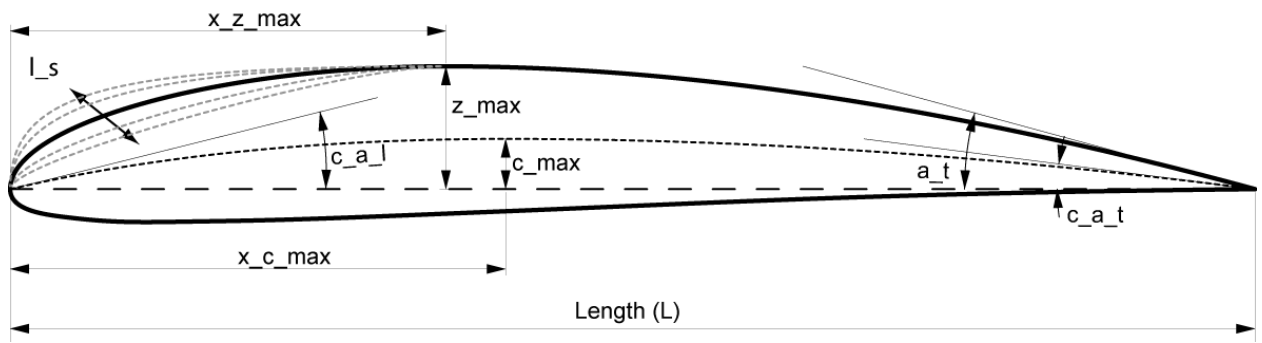


Figure 3.1.1.1: Airfoil parameters

Table 3.1.1.1: Parameters of camber curve and its abbreviations

Parameters	Abbreviations
Leading edge angle	$c_{a_l}$
Trailing edge angle	$c_{a_t}$
Maximum camber width	$c_{max}$
Longitudinal position of maximum camber width	$x_{c_{max}}$

The camber curve construction is divided into two parts for simplicity in network construction and airfoil parameters are represented in Figure 3.1.1.1.

Its first part is build using point 1, point 2 and point 3. To give clear explanation, components of Grasshopper® will be introduced step by step. Component *Point* is used here to define the points in X, Y and Z coordinates. However, airfoil shape only needs X and Y coordinates. Point 3 indicates the coordinates of the max width of the curve, ( $x_{max}$ ,  $y_{max}$ ). The values of  $x_{max}$  and  $y_{max}$  are set using component *Number Slider*. Component *Number Slider* has numeric upper and lower limit. Then it goes to *Remap Numbers* component in order to remap numbers. For  $x_{max}$ , target domain is from 0.2 to 0.8. For  $y_{max}$ , it is from 0.01 to 0.15. *Remap Numbers* component is used to define angles and points directly. Point 2 is located at ( $x$ ,  $y_{max}$ ), where  $y_{max}$  is set by user using *Numeric Slider*,  $x$  is expressed as  $y_{max}/\tan(\text{leading\_edge\_angle})$ . The intermediate control point needs to be at the intersection of two lines: a horizontal line passing through point 3 and the line passing through point 1 with an angle equal to the leading-edge angle. Here, the leading-edge angle is defined by *Numeric Slider* with numeric domain from 0 to 1. Then, it also goes to *Remap Numbers* component with target domain calculated via *Expression*:  $\text{atan}(y_{max}/x_{max})$ . Therefore, leading edge angle directly depends on the values of  $x_{max}$  and  $y_{max}$ . As a result, model is

constructed. Few manipulations with the building blocks and its connections allows us to establish such relationships that when any of the parameters are changed the control points 2 and 3 change accordingly.

The second part of the camber curve is modeled with the aid of 3 control points: point 3, point 4 and point 5. While point 3 and 5 are already defined, point 4 is defined as the point 2. It is located at  $(x, y_{max})$  where point  $x$  can be found as  $1 - y_{max}/\tan(\text{trailing\_edge\_angle})$ . Because, this point is located in the second part of the curve. The intermediate control point needs to be at the intersection of two lines: a horizontal line passing through point 3 and the line passing through point 5 with an angle equal to the trailing edge angle. Trailing edge angle is determined by method similar to leading edge angle determination. However, when it is remapped into a new numeric domain, its target domain calculated using another *Expression*:  $\text{atan}(-y_{max}/(x_{max}-1))$ . *Set Union* component is used to create a union of defined control points. For the first part of camber curve, point 1, point 2 and point 3 are set together. For the second part, point 3, point 4 and point 5 are joined. Hence, two parts of camber curve are constructed using component *Nurbs Curve* that requires curve degree insertion. In our case, it is set to two degrees, because there are 3 control points for each curve. Finally, *Join Curves* component is used to join two curves and get camber curve. Figure 3.1.1.2 illustrates the camber curve construction algorithm in Grasshopper. Figure 3.1.1.3 illustrates the curve itself in Rhinoceros because of constructed model.

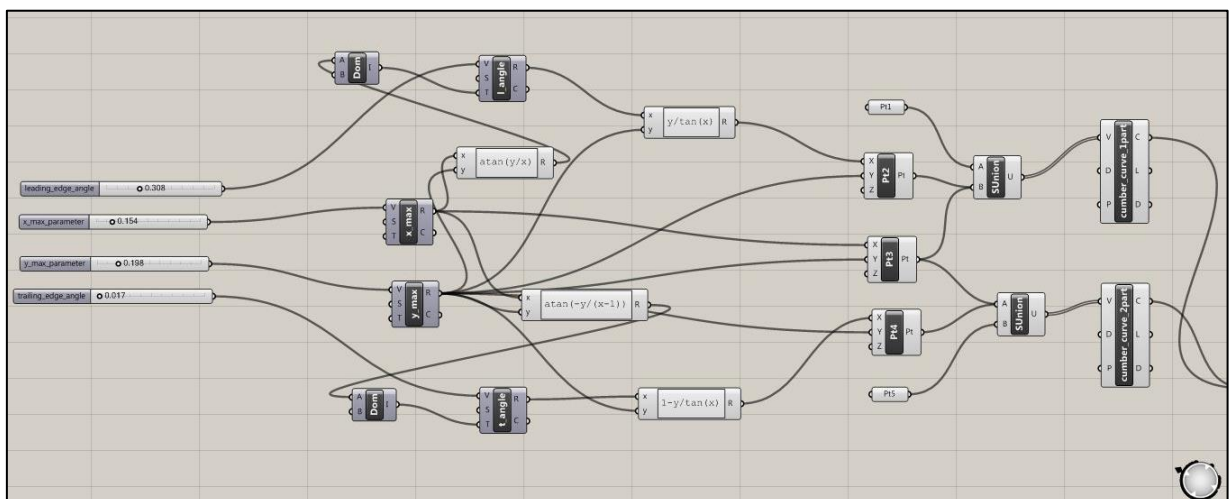


Figure 3.1.1.2: Construction algorithm of camber curve in Grasshopper® software

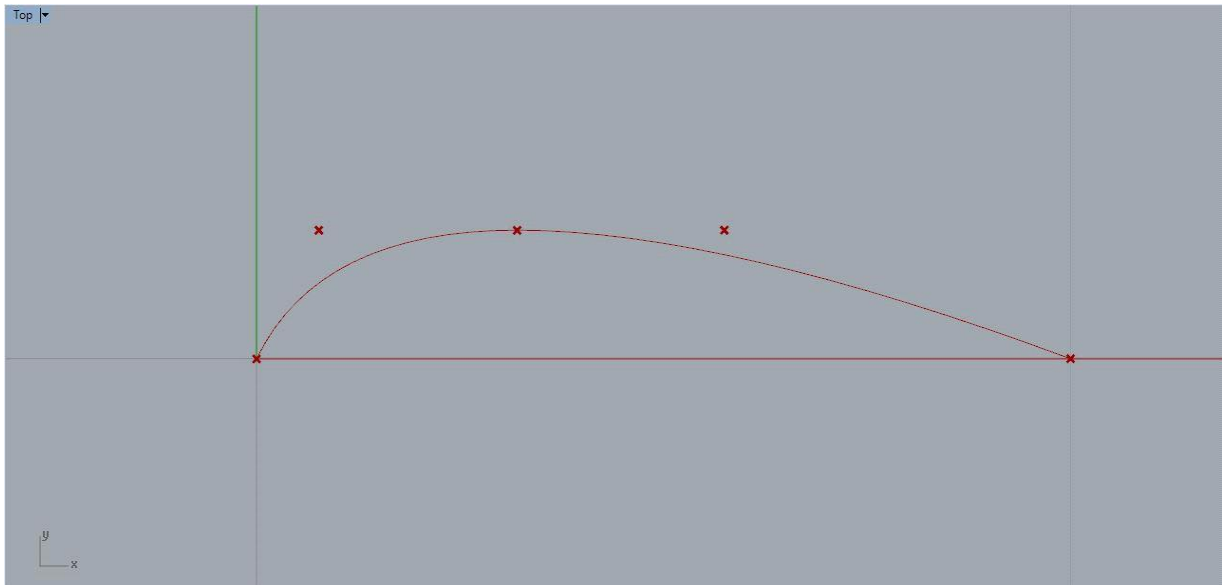


Figure 3.1.1.3: Camber curve in Rhinoceros software

### 3.1.2. Upper Curve

The design construction of upper curve is similar to camber curve. Upper side is also divided into two parts for simplicity. Second part is designed as the tail of the camber curve, while the first part has some alterations. Tail part of upper curve is also two-degree curve, while the first part of the curve is different. It is modeled with the aid of 4 points; therefore, it is a third-degree curve. It can be observed from Figure 3.1.1.1.

Table 3.1.2.1: Parameters of upper curve and its abbreviations

Parameters	Abbreviations
Leading edge angle	$l_s$
Trailing edge angle	$a_t$
Maximum camber width	$z_{max}$
Longitudinal position of maximum camber width	$x_{z_{max}}$

Point 1 (0,0) and point 6 (L,0) are fixed. Point 4 define the coordinates of the max width of the curve, ( $x_{max}$ ,  $y_{max}$ ). Points 2 and 3 are used to designate the nose of upper curve. *Numeric Slider* component expressed as  $ls_{parameter}$  helps to change the position of points in conjunction. Moreover, the leading edge of upper curve is 90 degrees at starting point 1. Point 2 is defined as (0, y), where y is calculated via

Expression  $1s\_parameter*y\_max$ . Point 3 coordinates are  $(x, y\_max)$ , where  $x$  is expressed through  $(1-1s\_parameter)*x\_max$ .

For the second part, point 5 is located at  $(x, y\_max)$ , where  $y\_max$  is set by utilizing *Numeric Slider*, while  $x$  is denoted as  $1-y\_max/\tan(\text{trailing\_edge\_angle})$ . Here, the trailing edge angle is defined by *Numeric Slider*. Then, it is remapped by *Remap Numbers* component using Expression:  $\text{atan}(-y\_max/(x\_max-1))$  for the target domain calculation. Consequently, control points 1, 2, 3 and 4 are united together in order to obtain first part of the upper curve (*Nurbs Curve* component with third-degree curve). Another union is produced by control points 4, 5 and 6 (*Set Union* component) to construct second part of the upper curve (*Nurbs Curve* component with two-degree curve). *Join Curves* component is used to define upper curve as one curve. Figure 3.1.2.1 interprets the upper curve Grasshopper® algorithm. Upper curve is represented in Figure 3.1.2.2.

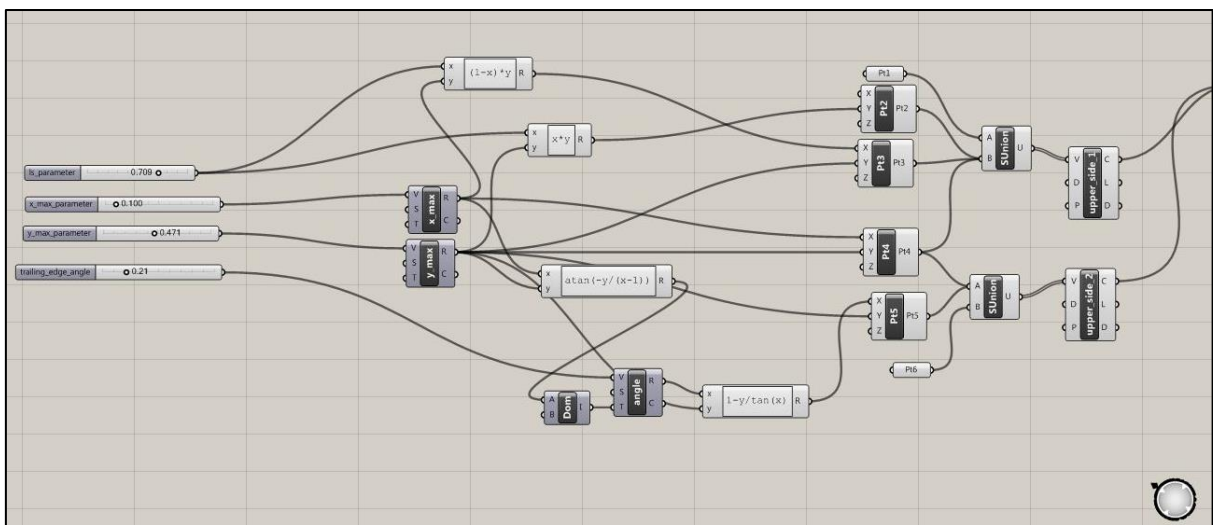


Figure 3.1.2.1: Construction algorithm of upper curve in Grasshopper® software

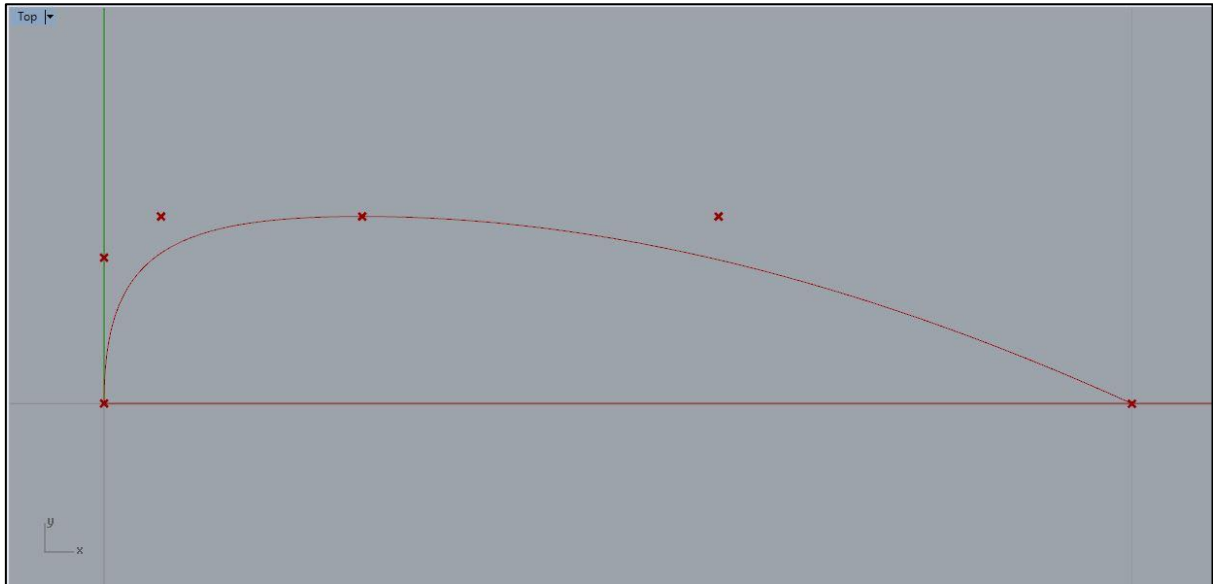


Figure 3.1.2.2: Upper curve in Rhinoceros software

### 3.1.3. Lower Curve

The construction of lower curve is based on the upper and camber curves. The main principle is to select specific number of points on the upper curve and mirror it about camber curve. Initially, *Divide Curve* component is used to divide a curve into equal length segments, thereby new points are appeared. Totally, 10 equal line segments are taken. Consequently, points on camber curve are detected through *Curve Closest Point* component. As a result, there is the same number of points on camber curve as on upper curve that are connected with those points identified on upper curve respectively using *Line* component. Afterwards, *Mirror* component is used which requires geometry to be mirrored and mirror curve. In our case, geometry and mirror curve are above-mentioned lines and camber curve respectively. In order to construct lower curve, end points of that mirrored lines are needed. *End Points* component helps to identify corresponding end points. As a result, new set of points defined which is used to construct lower curve of the airfoil using *Interpolate (t)* component. Here, the importance of constructing camber curve is characterized. Also, the leading edge angle of lower curve is 90 degrees, which can be directly set through limits of the component *Interpolate (t)* (Tangent at start of curve  $\{0.0, -1.0, 0.0\}$ ). Finally, joining upper, camber and lower curves constructs 2D airfoil shape that is represented in Figure 3.1.3.2 below.



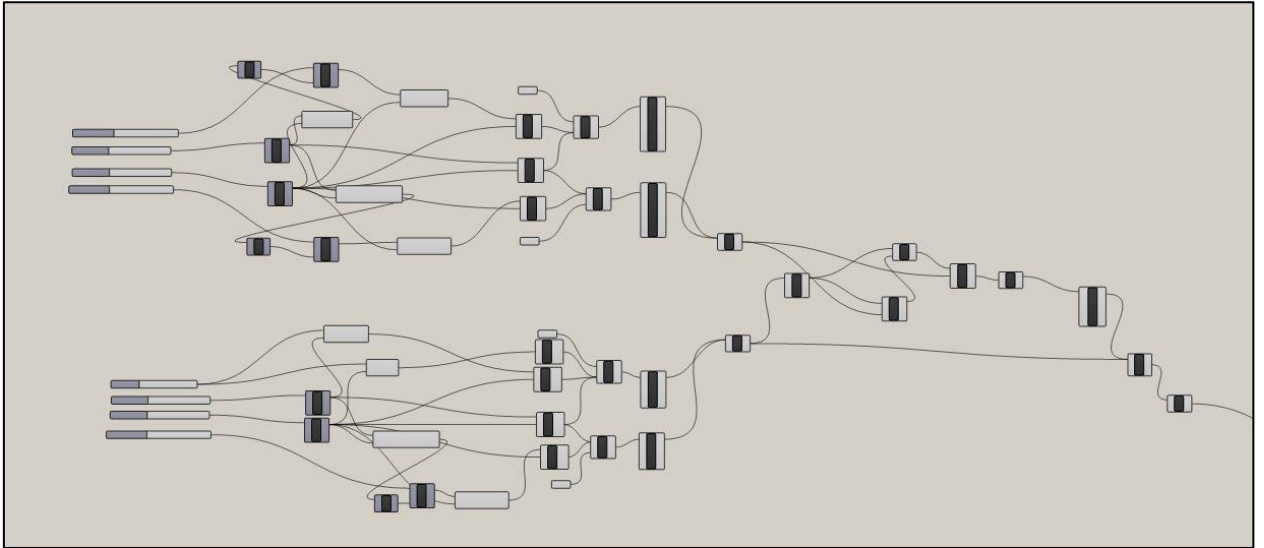


Figure 3.1.4.1: Airfoil algorithm

### 3.1.5. Read File component

The aim of *Read File* component is to read corresponding parameters from external sources such as notepad text editor, wordpad and so on. Hence, this component can be used instead of above-mentioned sliders in order to simplify the insertion procedure of parameters. Parameters are taken from internet or reliable sources can be further transported into some text editor. Then, using *Read File* component instead of *Numeric Slider* component to read the file, shape and surface construction can be developed in an automated manner.

### 3.2. Blade Surface Definition

In the proposed philosophy, the blade surface definition depends on progressive 2D airfoil profiles. The relating blade cross-sections (airfoil shapes) are determined by a direct interpolation process through a set of points, utilizing the curve fitting technique. The derived curves are distributed in perpendicular planes along a line, which establishes the pitch axis of the blade. The twist of the blade depends on twist angle of each cross-section. By applying the appropriate translational and rotational motions the section curves are accordingly positioned in the 3D space.

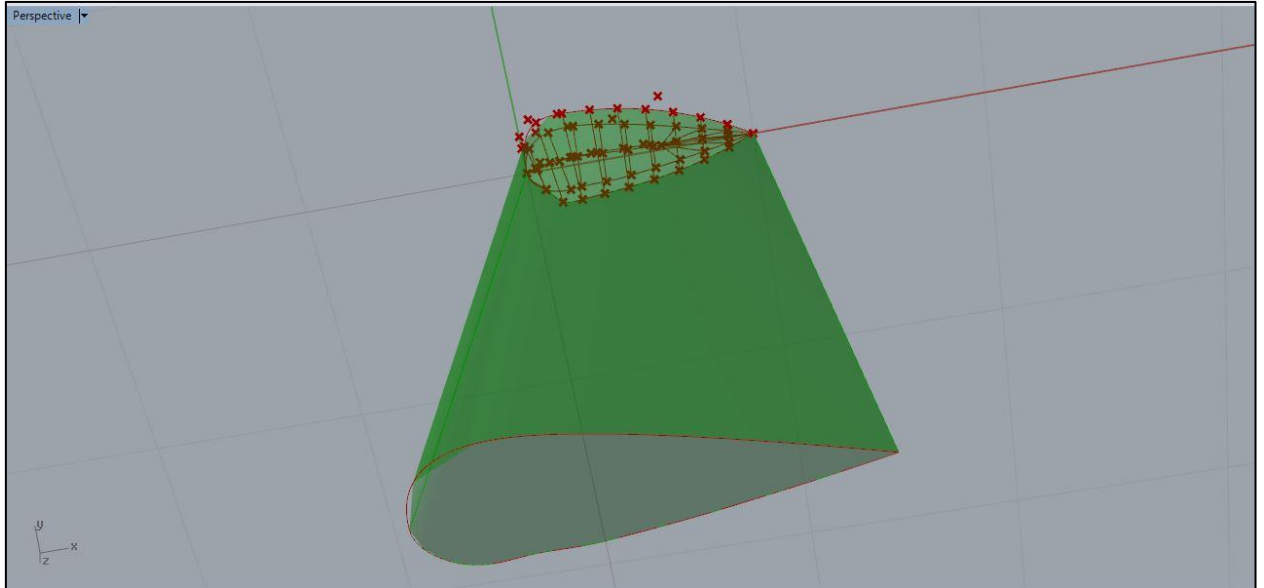


*Figure 4.1.1: Blade construction in 3D space*

Once the airfoils are properly arranged, the construction of blade surface can be performed by using the built cross-sections. Grasshopper® gives the ability to make surfaces through different methods; in the present work, the surface is described using the lofting method. To succeed this, each cross-section is formed as single NURBS curves to avoid discontinuity issues in the resulting surface. An illustration plan of a 3D surface is displayed in Figure 4.1.1.

### **3.3. Geometry Description**

The geometrical coordinates for NREL's S809 Airfoil 150-400 kW wind turbine was used to show the flexibility of introduced methodology. The geometrical data of airfoil used are taken from the work of Somers [8]. S809 Airfoil shape is shown in Figure 4.2.1. S809 Airfoil coordinates, namely upper curve and lower curve points are represented in table 1.

These points are utilized to show the performance of generated methodology. The main aim is to import S809 Airfoil points of upper and lower curves into Rhinoceros program. Then using airfoil algorithm, airfoil shape should be manipulated so that it

corresponds to S809 Airfoil shape by changing different parameters in Grasshopper® using sliders. This process is illustrated in Figure 4.2.2.

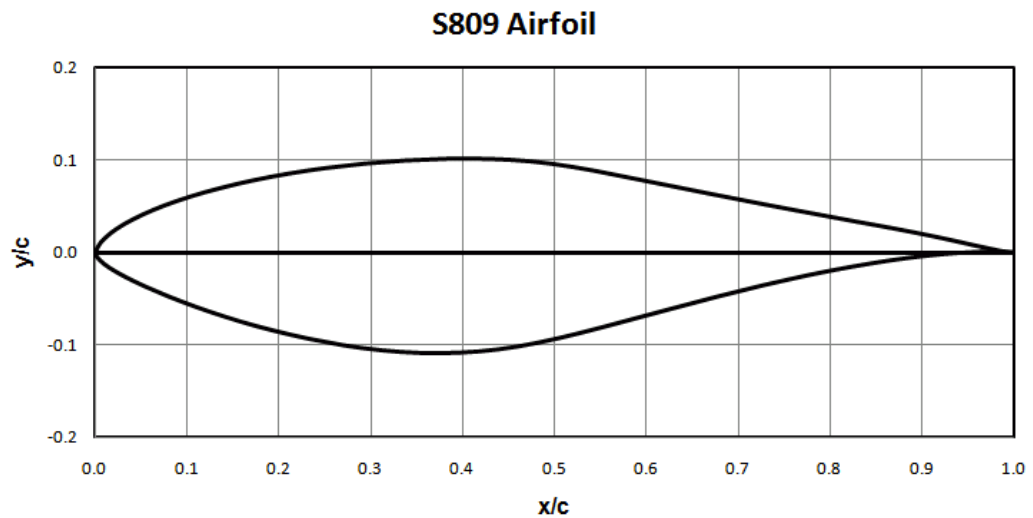


*Figure 4.2.1: S809 Airfoil shape*

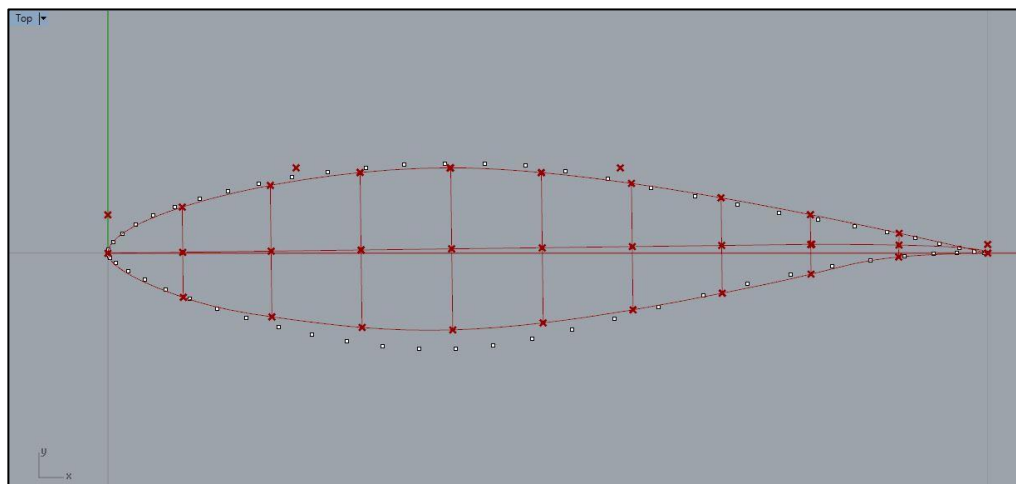


*Figure 4.2.2: S809 Airfoil points and produced airfoil*

## 4. ANSYS FLUENT SIMULATION

### 4.1. Description of Tool

This research utilizes the software FLUENT by ANSYS to analyze the flow. This flow modeling software provides expansive modeling abilities necessary to model flow, turbulence, heat transfers and range of reactions for practical applications ranging from the air flow around the wing to combustion in a heater. Its technology enables quick and accurate CFD results, adaptable meshes and unrivaled parallel scalability. Besides,

ANSYS allows import of meshes from other softwares. Utilizing the functionality, offered 2D airfoils and 3D blades can be efficiently analyzed. Progresses and innovations in modern technology and software developments have revolutionized the whole engineering design process of products. There is a substantial number of quality CFD packages that can be used to model flow over solid objects. The modeling procedure consists of few steps. Initially, the geometry and meshes are created. After the development of the mesh or grid, a solver is utilized to solve the governing equations of the problem. FLUENT has been chosen as our main solver during this research. The results of the analysis were compared with the available data on NACA 4412 airfoil.

#### **4.2. Inputs and Constraints**

The mesh that will be created prior to the calculations will be on a structured domain. In Fluent, standard sea level values will be assumed for the freestream properties. Hence, Pressure = 101,325 Pa, Density = 1.176674 kg/m<sup>3</sup>. Temperature = 300 K Kinematic viscosity = 1.407e-5 m<sup>2</sup>/s. Chord length = 1m. Re=1000000. The freestream velocity will be 15.2 m/s and the angle of attacks analyzed are 0°, 1°, 3°, 5°.

#### **4.3. Simulation Procedure**

For the simulation procedure, the geometry of NACA 4412 airfoil was generated by our methodology using Grasshopper and Rhinoceros. Afterwards it was imported to ANSYS Workbench. The procedure of Fluent simulation is presented step by step in the next sections.

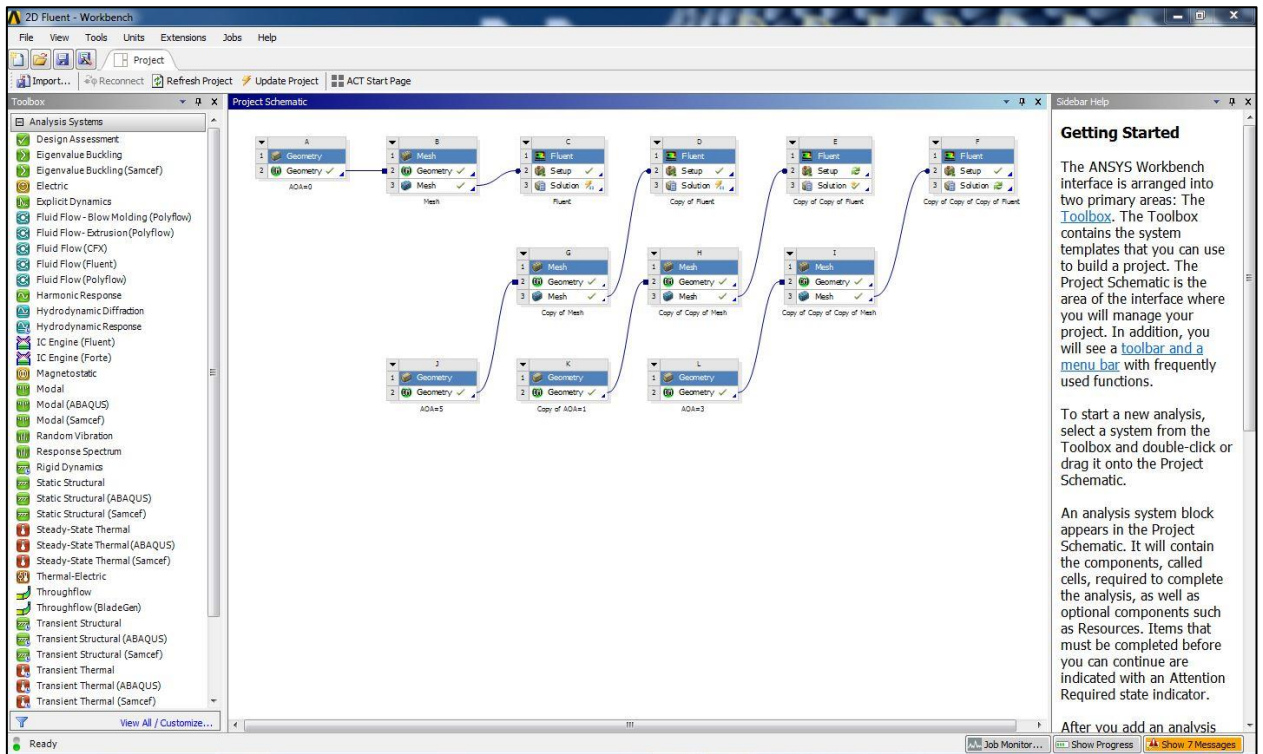


Figure 4.3.1: Whole procedure in ANSYS Workbench

The two-dimensional version of ANSYS Fluent was utilized, introducing the steady implicit coupled solver. It provides with the direct solution of continuity, momentum and energy equations at once. Pressure far-field boundary conditions were gauge pressure of 101,325 Pa and temperature of 300 K. In the turbulence model, default settings were utilized, with only change of turbulent viscosity ratio to 1 and turbulent intensity to 10%. For the solver, the modified turbulent viscosity was set to a second-order upwind discretization scheme.

#### 4.3.1. Turbulence Model

Inviscid flow analyses can be used when the effect of viscosity is negligible. For example, it is applied for high-Reynolds-number cases where inertial forces tend to dominate viscous forces. In case of an aerodynamic analysis of some high-speed projectile, the pressure forces on the body dominate the viscous forces. Therefore, an inviscid analysis provides a quite adequate estimate of the primary forces acting on the body. Once the shape of the body is improved to maximize the lift forces and minimize

the drag forces, a proper viscous analysis can be used to include the effects of the fluid and turbulent viscosity on the lift and drag forces[4].

Additional example when inviscid flow analysis can be performed is to obtain an adequate initial solution for problems involving complicated flow physics and/or complicated flow geometry. In this case, viscous forces are ignored at the initial stages in complicated momentum equations. But once the calculation has begun and the residuals are deminishing, the viscous terms are to be turned on by enabling laminar or turbulent flow and the solution to be progressed to converge. This is quite common method for complicated flows analysis.

#### **4.3.2. Geometry**

Firstly, we import the NACA 4412 airfoil shape to ANSYS Workbench Design Modeler from Rhinoceros. Afterwards, wind tunnel geometry was prepared appropriately as shown in figure. To get more accurate meshing, circle was drawn around an airfoil geometry. Moreover, rectangle was used to represent the path after wind passes the airfoil shape. It also increases the quality of mesh. The *Split Edges* feature was used, which allows for the splitting of edges into two or more pieces. In our case, it was divided into two parts. The last procedure in Design Modeler is to identify boundary conditions by creating named selections. They are: inlet, outlet, free, part1-airfoil, part2-airfoil.

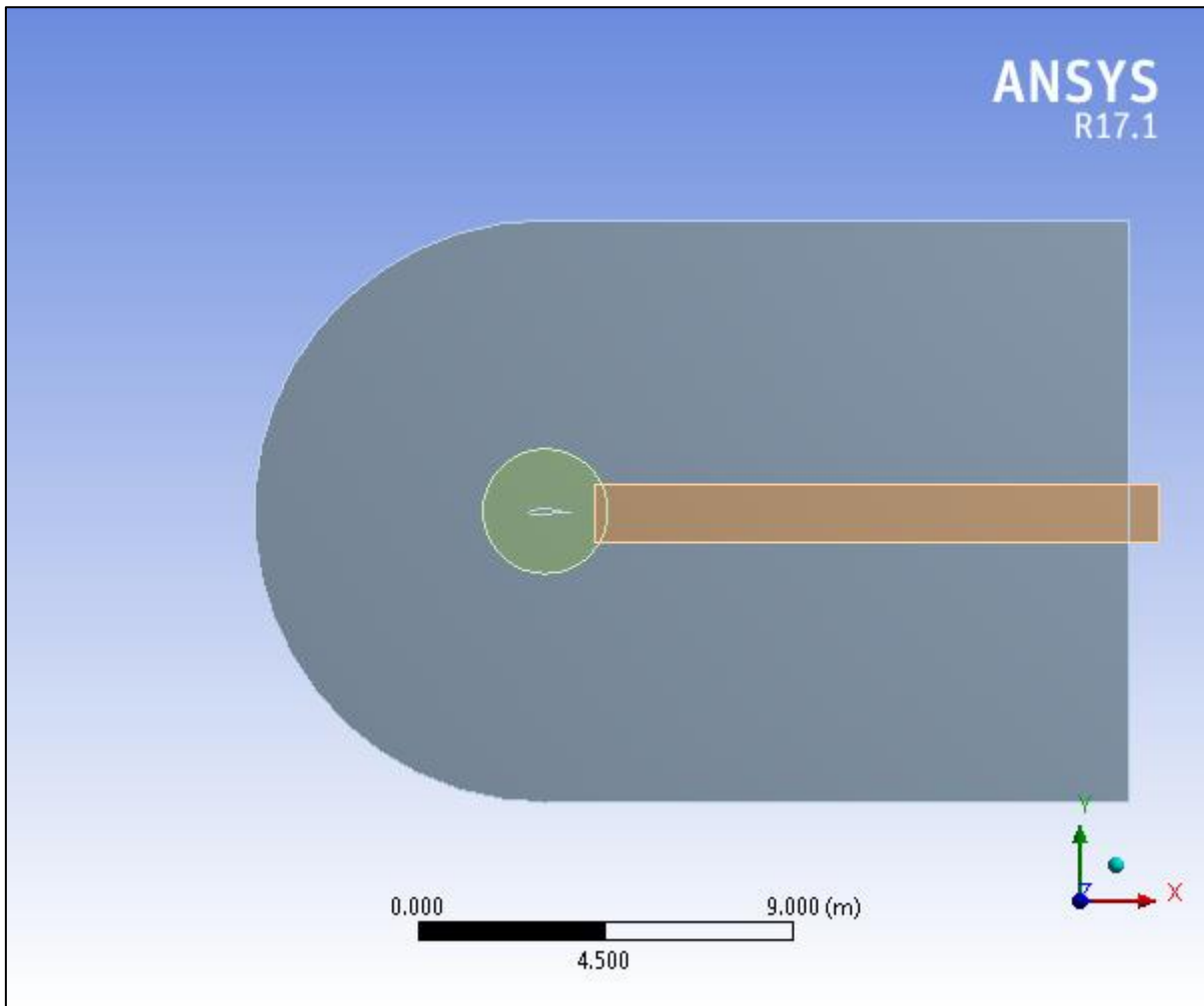


Figure 4.3.2.1: Geometry of a wind tunnel and airfoil at an angle of  $0^\circ$

### 4.3.3. Mesh Control

Meshing is the process in which the geometry is discretized into elements and nodes in space. The mathematical representation of the stiffness and mass distribution of the structure is done through meshing and material properties specification.

In ANSYS, the mesh can be set by default at a solve time, depending on several factors such as model size, the closeness of other topologies, curvature of the body, and complexity of the function. The fineness of the mesh can be varied to get more accurate results, or any can refine the mesh in the proximity of geometry where it is more important and leave the rest unchanged.

The mesh can be previewed before solving. Mesh controls like Global Mesh Controls, Local Mesh Controls, Virtual Topology are available in ANSYS to help the user in mesh adjustment [1].

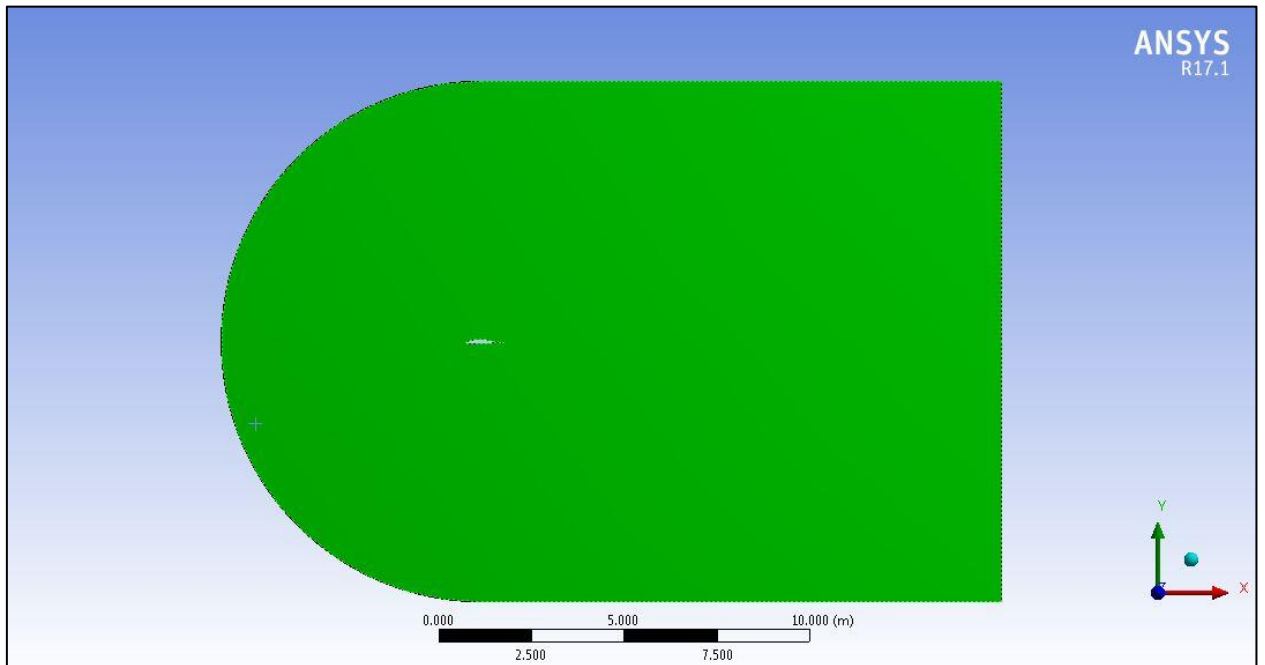


Figure 4.3.3.1: Wind tunnel at an angle of  $0^\circ$

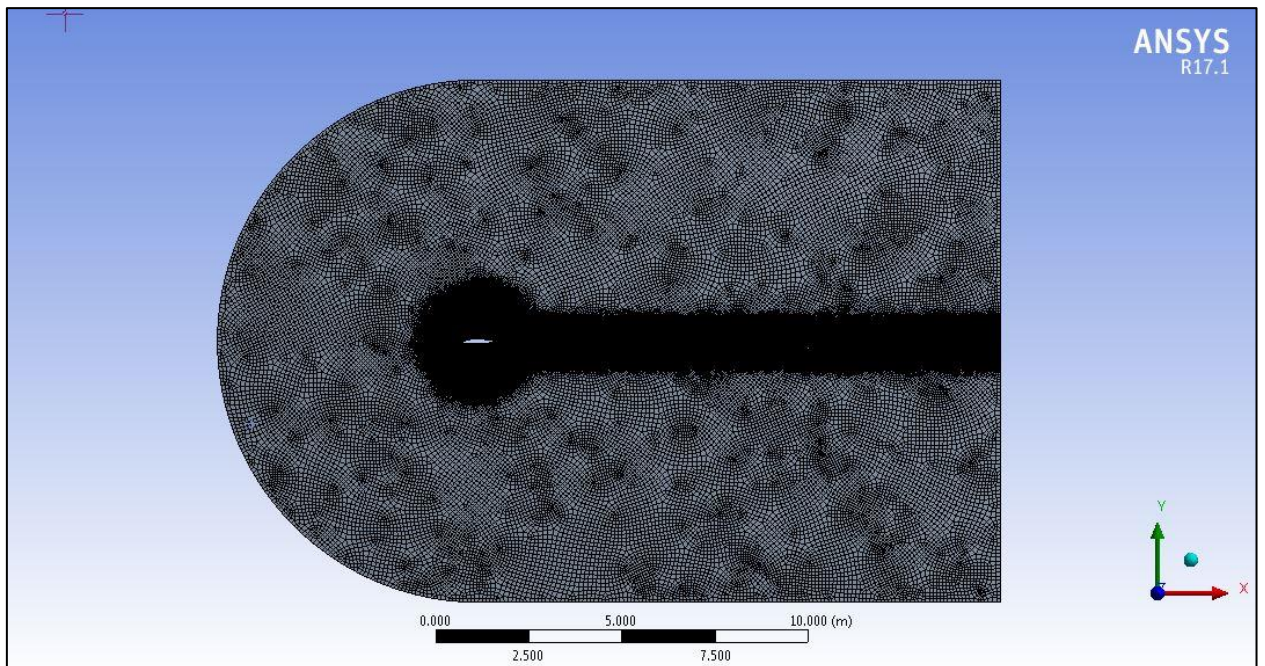


Figure 4.3.3.2: Mesh of a wind tunnel at an angle of  $0^\circ$

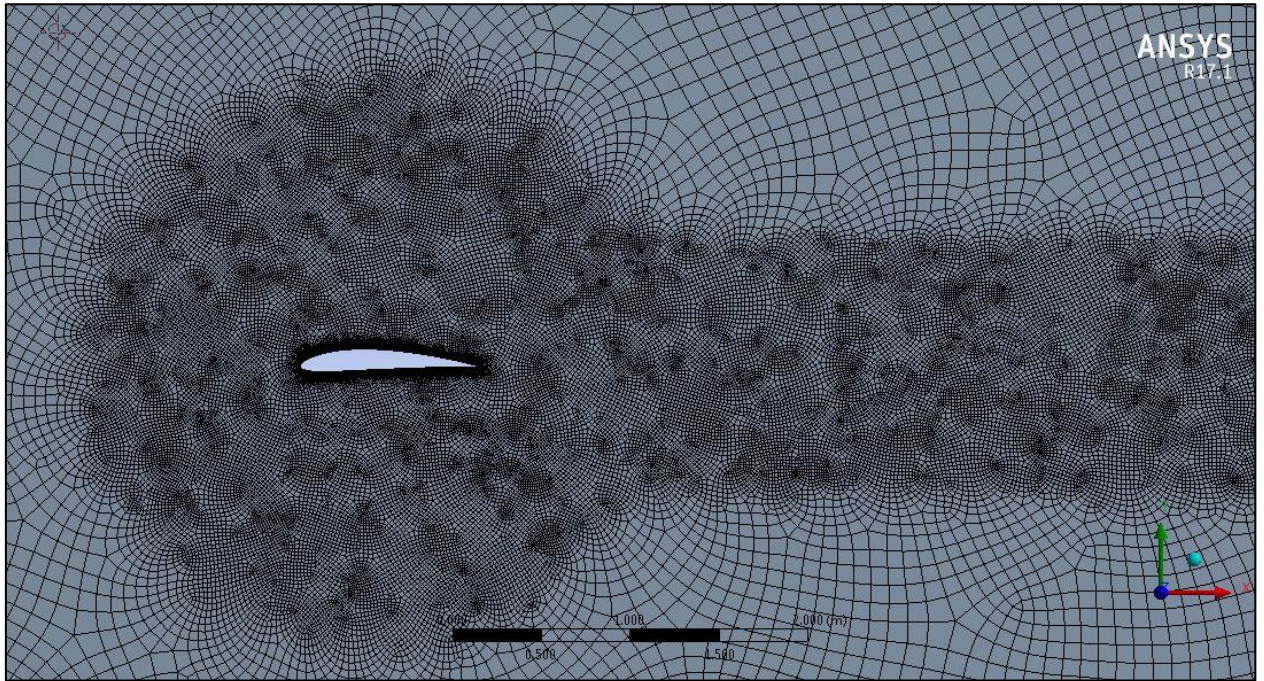


Figure 4.3.3.3: Scaled mesh of an airfoil at an angle of  $0^\circ$

Considering a 3D body, we start by choosing the body in which the inflation mesh will be created, and then recognise the faces that we want to inflate from.

For a swept body, we start by choosing the source face, and afterward the boundaries or edges from which it will be inflated. This is an alternate approach from other 3D bodies as the source face is meshed first individually, which is then swept through the body.

Once we have determined the boundaries of inflation, other parameters such as number of inflation layers, inflation growth rate can be managed easily by using different methods. They are *Total Thickness*, *First Layer Thickness*, *First layer Aspect Ratio*, *Last Layer Aspect Ratio* or the *Smooth Transition* option. In our case, *Total Thickness* option was used, which allows to set the exact number of inflation layers and growth rate. Inflation results are shown in figure 4.3.3.4.

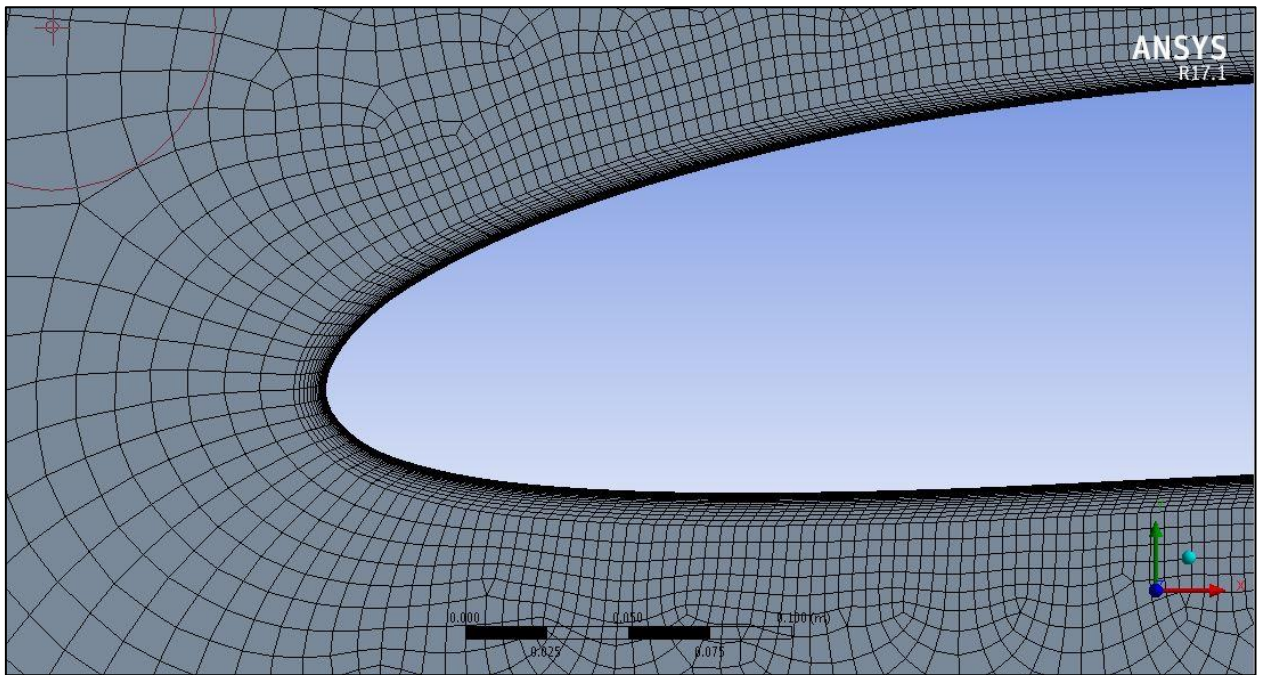


Figure 4.3.3.4: Inflation of an airfoil mesh at an angle of  $0^\circ$

Edge Sizing controls can be given to any edge and use bias factors, whereby the mesh size can be changed along the edge. Edge Sizing was used in two edges of airfoil. Furthermore, Edge Sizing has several options: specified element size, a number of divisions along the edge and sphere of influence. Number of divisions option was utilized by setting the division number to 250 for every edge.

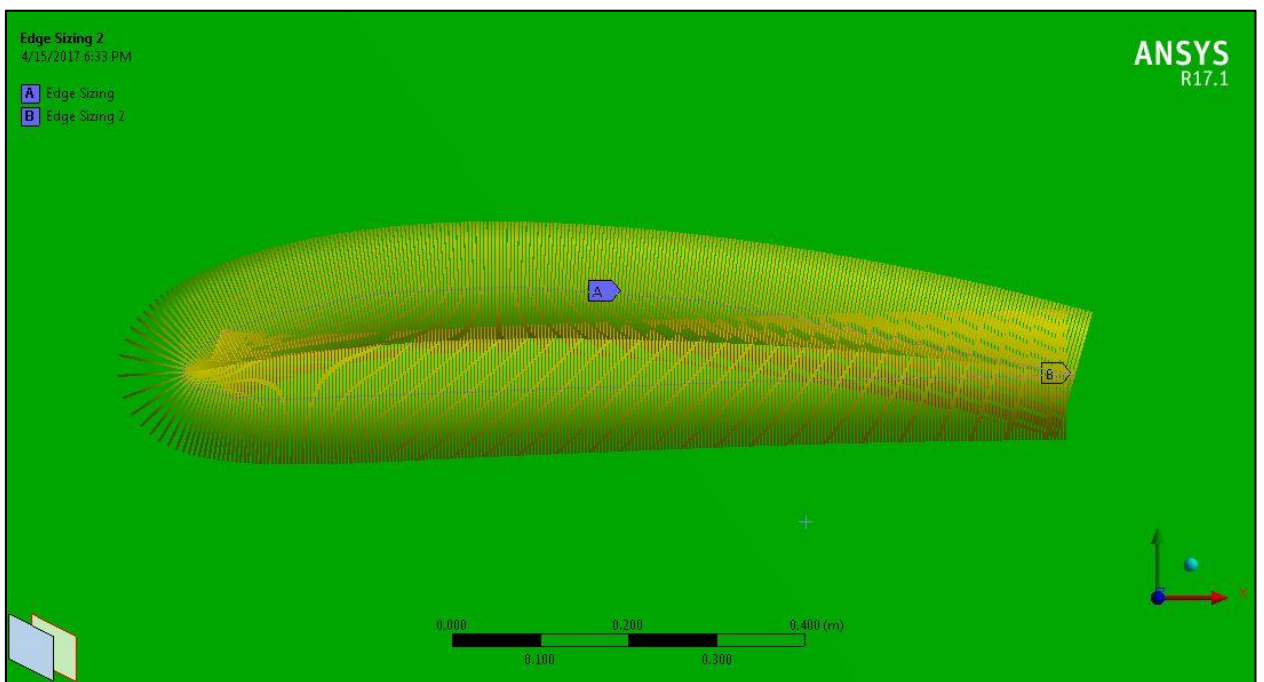
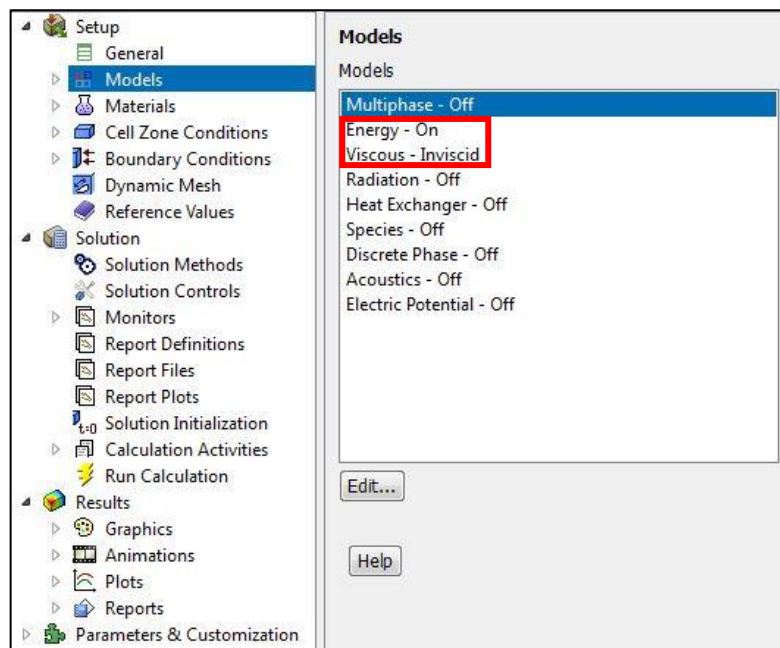
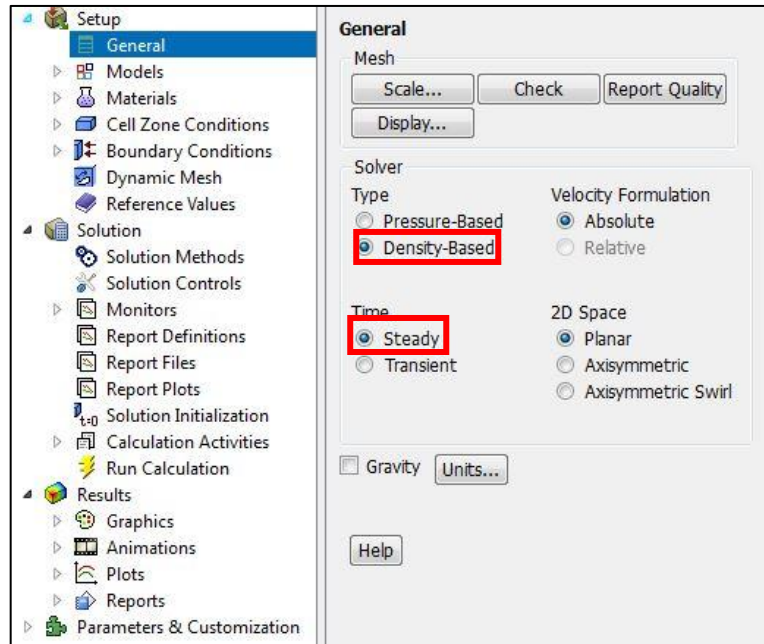
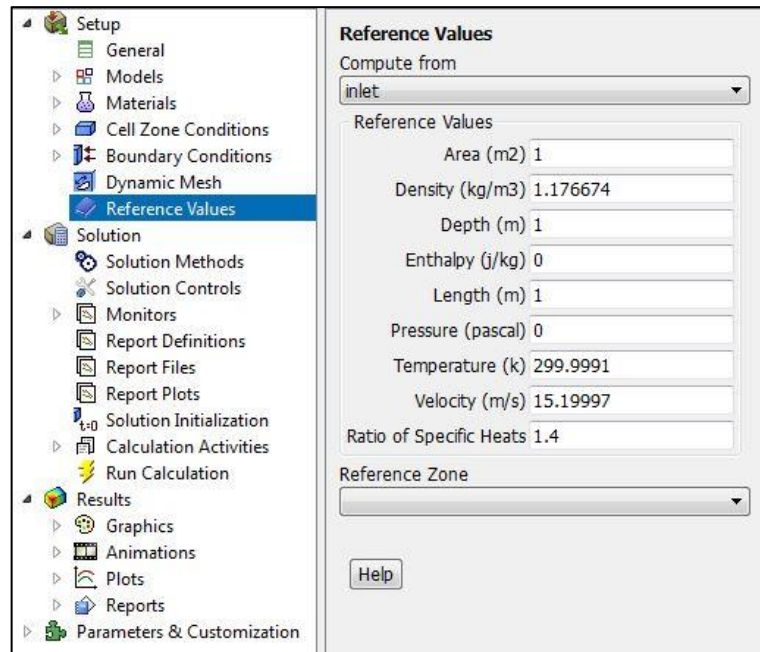
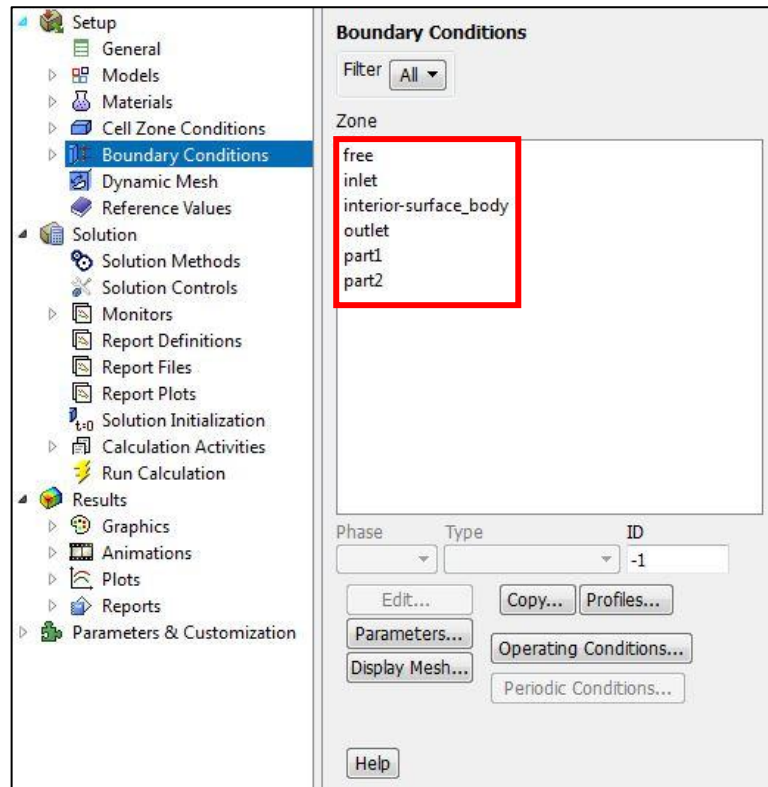
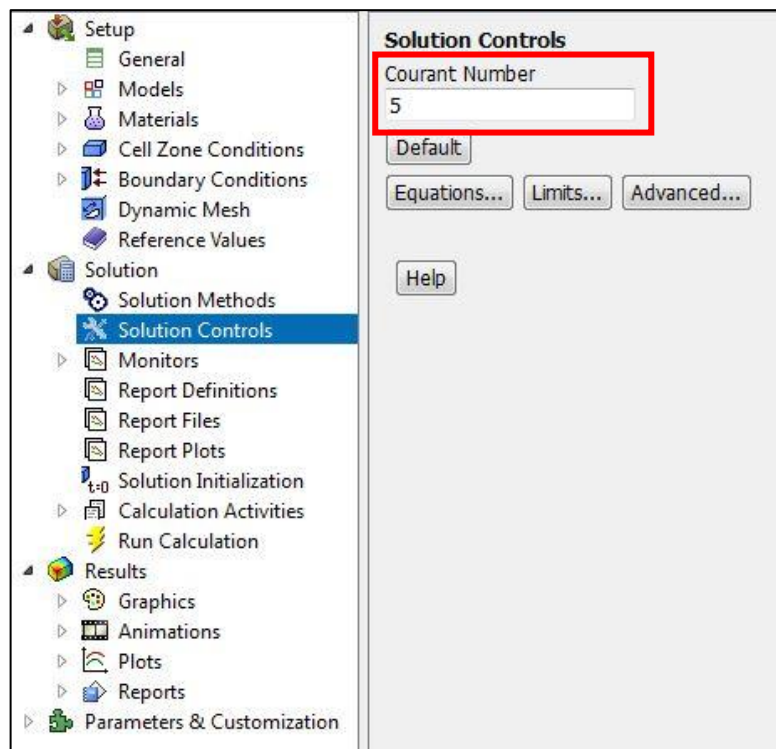
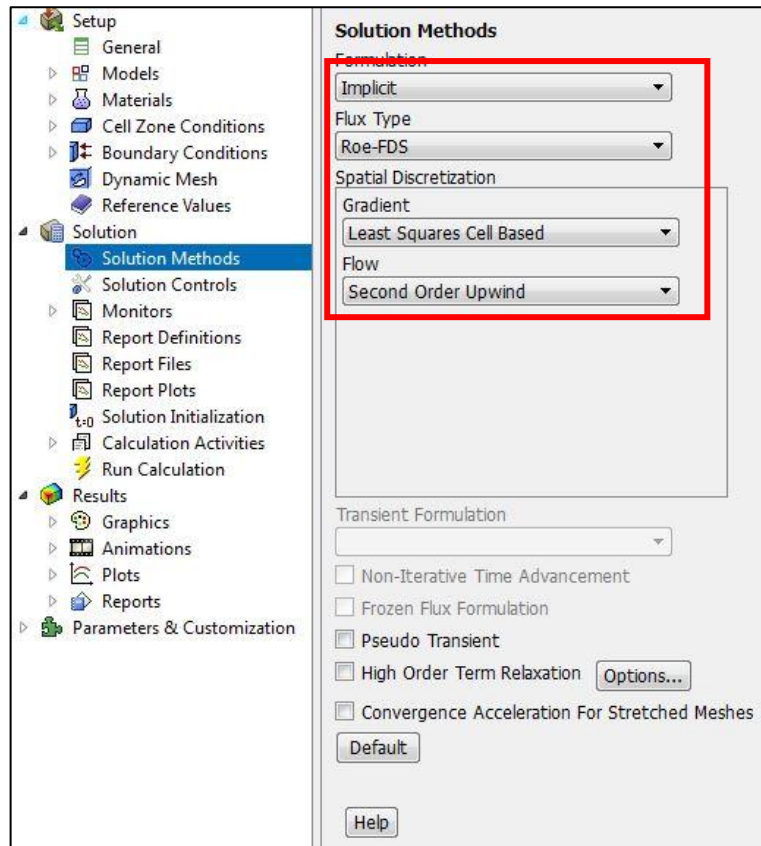


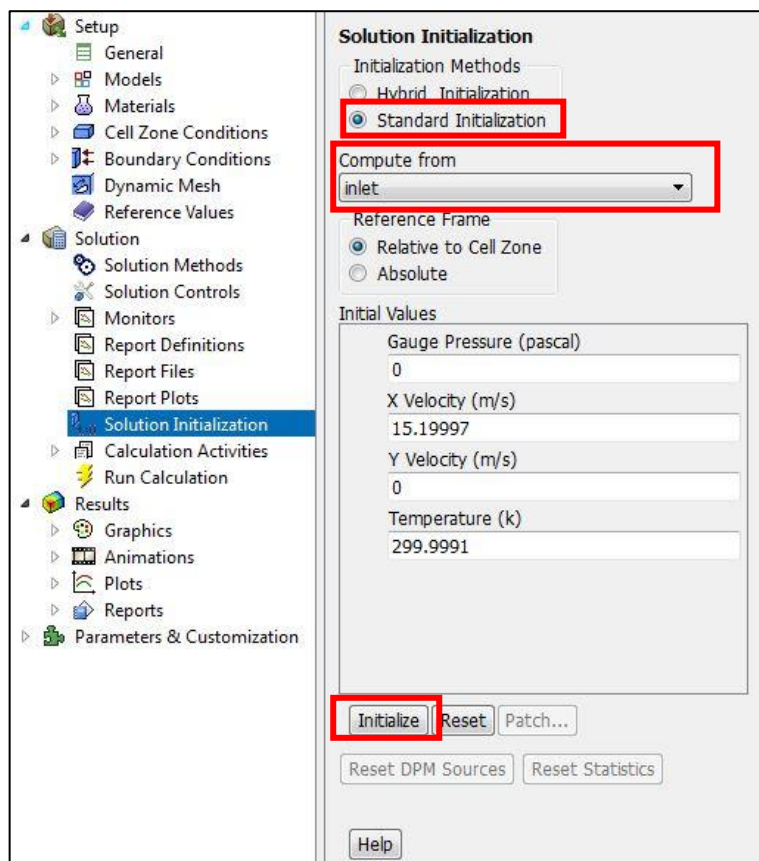
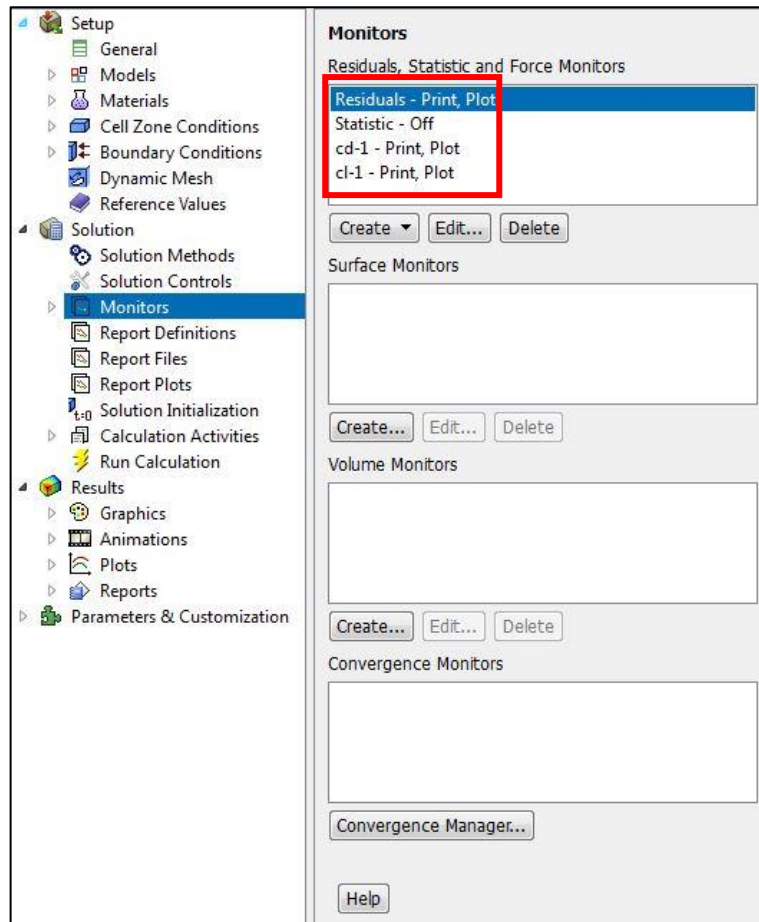
Figure 4.3.3.5: Edge sizing of an airfoil edges at an angle of  $0^\circ$

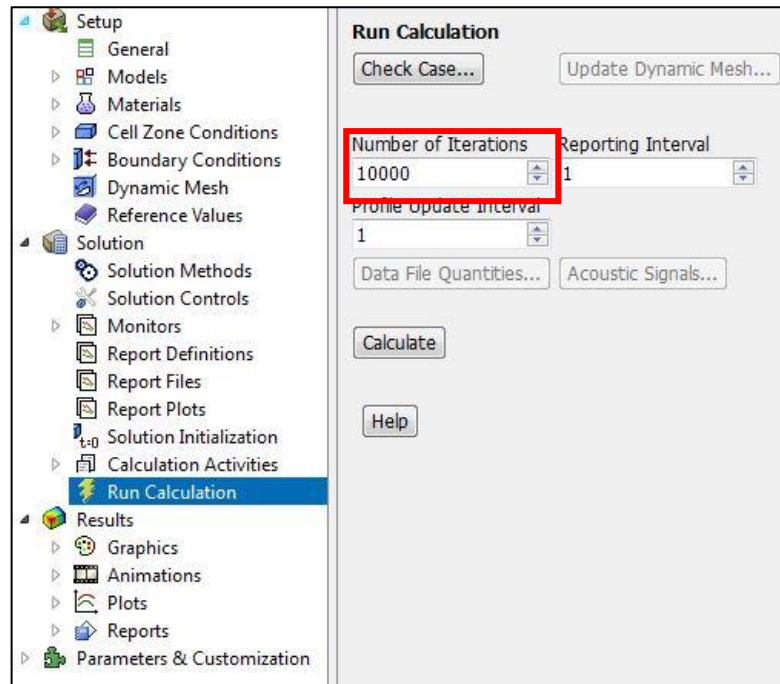
### 4.3.4. Set Up Procedure











## 5. OPTIMIZATION EXAMPLE

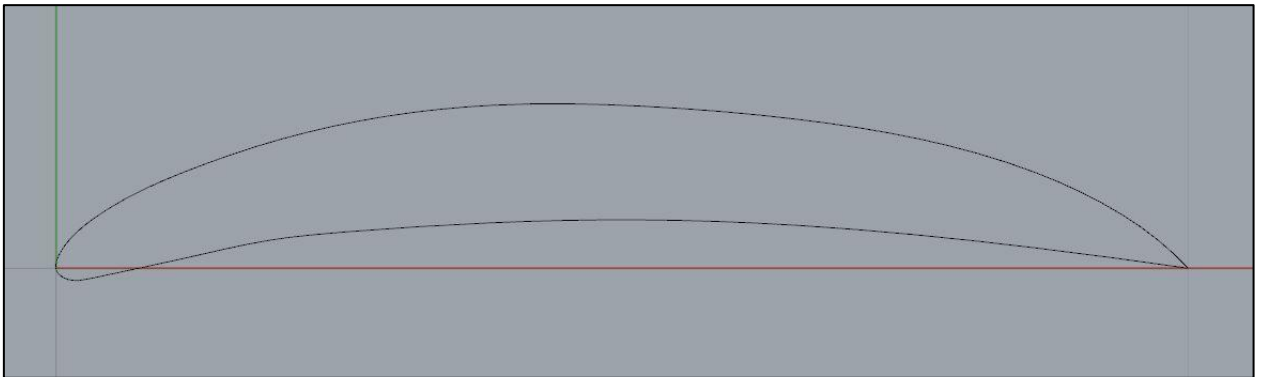


Figure 5.1: Shape of optimized airfoil

A maximization problem was setup where the optimization goal was to maximize the ratio of lift coefficient to drag coefficient ( $\frac{C_L}{C_D}$ ) under a specific area constraint. In the optimization loop, an inviscid potential flow solver, employed with one way-coupled boundary corrections, was used [16]. Our developed parametric model was used in the generation of different shapes as described in the corresponding section. The airfoil area was set to be equal to that of NACA 4412 airfoil area. The optimization algorithm employed was an evolutionary one (MATLAB's Genetic Algorithm implementation)

and the airfoil shape depicted in Fig. 5.1 was the resulting shape after around 6500 iterations. The same profile was also simulated in ANSYS Fluent using the same methods, options and set up procedure as in the simulation process of NACA 4412 airfoil we have previously mentioned. The primary purpose of this was to verify the optimization results by comparing them with ANSYS output.

Table 5.1: Inviscid solver and ANSYS Fluent results

<i>Inviscid solver</i>	$C_L=2.138465$	$C_D=0.014859$	$C_L/C_D \sim 144$
<i>ANSYS Fluent</i>	$C_L=1.995200$	$C_D=0.010635$	$C_L/C_D \sim 187$

The results from ANSYS are giving a higher lift over drag ratio but qualitatively and judging from the resulting shape and the good agreement in lift estimation we feel that we have a good indication that the optimizing framework works quite well.

Obviously, future work should include further experimentation with ANSYS simulations and realization of an optimization loop having ANSYS as the main flow solver.

## 6. RESULTS

Table 6.1: Results of ANSYS FLUENT simulation

Angle of attack (AOA)	$C_L$	$C_D$
0°	5.1021e-01	7.9353e-03
1°	6.3709e-01	6.4180e-03
3°	8.6788e-01	6.3324e-03
5°	9.6436e-01	8.5923e-03

Following the simulation procedure, finally we got the results which are shown in table 6.1. All data provided are computed with a help of convergence study, so that it provides more accurate results. For 0° angle of attack, the lift coefficient is 0.51021, while the drag coefficient is 0.0079353. For the rest of AOA, the simulation procedure was

changed with adding *Rotate* option in Design Modeler. Consequently, the desired angle of attack was achieved by rotating whole airfoil. For 1° angle of attack, the lift coefficient is 0.63709, while the drag coefficient is 0.006418. For 3° angle of attack, the lift and drag coefficients are 0.86788 and 0.0063324 respectively. The lift and drag coefficients are 0.96436 and 0.0085923 respectively for the 5° angle of attack.

## 7. CONCLUSION AND DISCUSSION

The aim of the work displayed in this report was to portray the advancement of an alternative model for the parametric geometry definition of wind turbine blade surface, utilizing the Grasshopper® graphical algorithm editor. The blade surface can be characterized in a direct and computerized way, by simply reading the parameters from external text files. 2D blade cross-sections are utilized for the development of the 3D NURBS surface through a lofting method. The utilization of introduced methodology demonstrated its effectiveness in description of blade surface and the procedure is comprehensible, which can be automatically re-shaped by simply changing their parameters, within pre-indicated limits.

Table 7.1: Data taken from *airfoiltool.com*

Alpha	Cl	Cd	Top_Xtr	Bot_Xtr
0	0.4833	0.00678	0.6232	0.4192
0.25	0.5102	0.00658	0.6101	0.5177
0.5	0.5366	0.00635	0.5975	0.6393
0.75	0.5622	0.00617	0.5856	0.7449
1	0.5842	0.00594	0.574	0.8717
1.25	0.6163	0.00588	0.5622	0.9842
1.5	0.6525	0.00598	0.5505	1
1.75	0.6788	0.00611	0.5398	1
2	0.7055	0.00622	0.5294	1
2.25	0.7325	0.00633	0.5204	1
2.5	0.7592	0.00646	0.5112	1
2.75	0.7865	0.00656	0.5029	1
3.25	0.8405	0.00681	0.4847	1
3.5	0.8672	0.00696	0.4746	1
3.75	0.8941	0.00709	0.4646	1

4	0.921	0.00722	0.454	1
4.25	0.9473	0.00739	0.4426	1
4.5	0.9734	0.00758	0.4273	1
4.75	0.9993	0.00778	0.411	1
5	1.0254	0.00797	0.3979	1

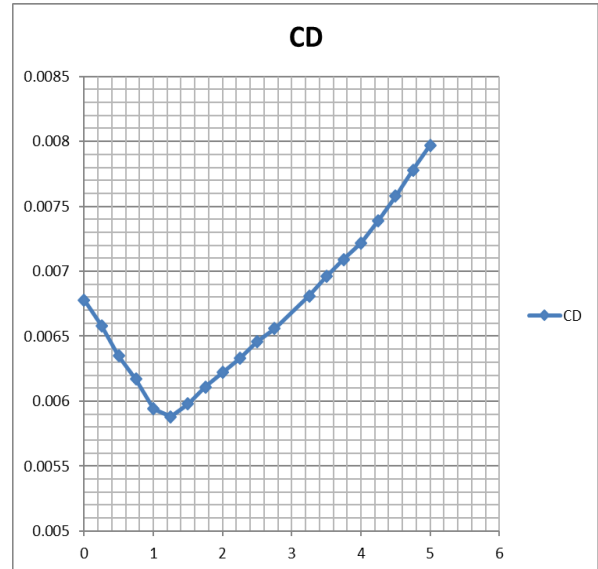
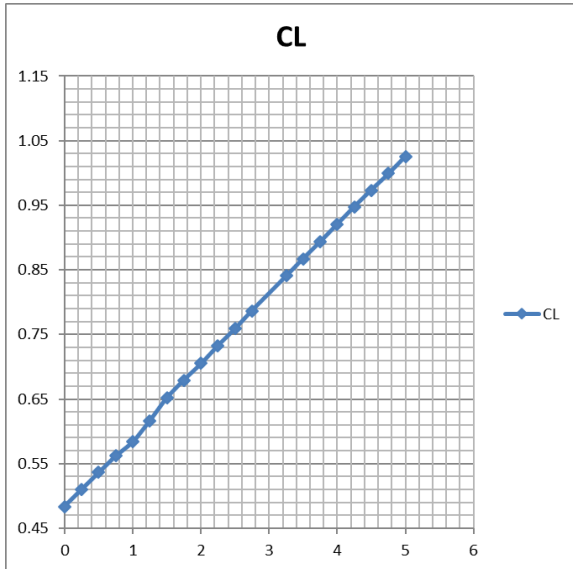


Figure 7.1:  $C_L$  coefficient data from airfoiltools.com

Figure 7.2:  $C_D$  coefficient data from airfoiltools.com

In this study lift and drag performances of NACA 4412 airfoil were performed. A FLUENT program was used to numerical calculations. Computational results presented in section 6 was compared with available data on NACA 4412 airfoil which is represented in table 7.1. The difference in percentage was given as follows:

- ❖ For  $0^\circ$  angle of attack: 5.57% for lift coefficient, 17.04% for drag coefficient
- ❖ For  $1^\circ$  angle of attack: 13.32% for lift coefficient, 8.05% for drag coefficient
- ❖ For  $3^\circ$  angle of attack: 6.68% for lift coefficient, 6.88% for drag coefficient
- ❖ For  $5^\circ$  angle of attack: 5.95% for lift coefficient, 7.81% for drag coefficient

By this method, the computational results agreed very well with corresponding experimental data.

## REFERENCE LIST

- [1] ANSYS, Inc. ANSYS Mechanical User's Guide. Release 15 (2013).
- [2] Charalampous, G. Kyriakos, Giorgos A. Strofylas, Geogios I. Mazanakis and Ioannis K. Nikolos. "Wind Turbine Blades Parametric Design Using Grasshopper". 8th GRACM International Congress on Computational Mechanics (2015).  
<http://8gracm.mie.uth.gr/Papers/Session%20D2-C3/K.%20Charalampous.pdf>.
- [3] Energy Data. Global Energy Statistical Yearbook (2016). <https://yearbook.enerdata.net>.
- [4] Eleni, C. Douvi, Tsavalos I. Athanasios and Margaris P. Dionissios. "Evaluation of the turbulence models for the simulation of the flow over a National Advisory Committee for Aeronautics (NACA) 0012 airfoil". Journal of Mechanical Engineering Research Vol. 4(3) (2012): 100-111. DOI: 10.5897/JMER11.074.
- [5] Gurit. Wind Turbine Blade Aerodynamics.  
<http://www.gurit.com/files/documents/2aerodynamicspdf.pdf>.
- [6] Hameed, M. Saqib and S. Kamran Afaq. "Design and Analysis of A Straight Bladed Vertical Axis Wind Turbine Blade Using Analytical And Numerical Techniques". Ocean Engineering 57 (2013): 248-255. doi: 10.1016/j.oceaneng.2012.09.007.
- [7] Noorazyze S, Noorazyze Z. "Performance Evaluation of Slotted and Continuous Types Wind Turbine Blade". (2014).
- [8] Pérez-Arribas, F. and I. Trejo-Vargas. "Computer-Aided Design of Horizontal Axis Turbine Blades". Renewable Energy 44 (2012): 252-260. doi: 10.1016/j.renene.2012.01.100.
- [9] Şahin, İzzet and Adem Acir. "Numerical and Experimental Investigations of Lift and Drag Performances of NACA 0015 Wind Turbine Airfoil". International Journal of Materials, Mechanics and Manufacturing 3 (2015): 22-25. DOI: 10.7763/IJMMM. 2015.V3.159.
- [10] Sederberg, W. Thomas. "Computer Aided Geometric Design". (2011).
- [11] Schubel, J. Peter and Richard J. Crossley. Wind Turbine Blade Design (2012).  
<https://pdfs.semanticscholar.org/02e3/4541848594efcf28fab409b2eef696fe145a.pdf>.
- [12] Song, Fangfang, Yihua Ni, and Zhiqiang Tan. "Optimization Design, Modeling and Dynamic Analysis for Composite Wind Turbine Blade". Procedia Engineering 16 (2011): 369-375. doi: 10.1016/j.proeng.2011.08.1097.
- [13] Somers, M. Dan. "Design and Experimental Results for the S809 Airfoil". National Renewable Energy Laboratory (1997).
- [14] Strofylas, G.A., Mazanakis, G.I., Nikolos, I.K. (2014), "Wind turbine blade structure parameterization using T4T". Proceedings of the ASME 2014 International Mechanical Engineering Congress & Exposition, IMECE2014, Nov. 14-20.
- [15] Qblade. En.Wikipedia.Org. (2016). <https://en.wikipedia.org/wiki/QBlade>.
- [16] Wauquiez, Christian. "Shape Optimization of Low Speed Airfoils using MATLAB and Automatic Differentiation". Royal Institute of Technology, Stockholm, Sweden (2000).

## APPENDICES

Table 1. S809 Airfoil Coordinates

Upper Surface		Lower Surface	
x/c	z/c	x/c	z/c
0.00037	0.00275	0.00140	-0.00498
.00575	.01166	.00933	-.01272
.01626	.02133	.02321	-.02162
.03158	.03136	.04223	-.03144
.05147	.04143	.06579	-.04199
.07568	.05132	.09325	-.05301
.10390	.06082	.12397	-.06408
.13580	.06972	.15752	-.07467
.17103	.07786	.19362	-.08447
.20920	.08505	.23175	-.09326
.24987	.09113	.27129	-.10060
.29259	.09594	.31188	-.10589
.33689	.09933	.35328	-.10866
.38223	.10109	.39541	-.10842
.42809	.10101	.43832	-.10484
.47384	.09843	.48234	-.09756
.52005	.09237	.52837	-.08697
.56801	.08356	.57663	-.07442
.61747	.07379	.62649	-.06112
.66718	.06403	.67710	-.04792
.71606	.05462	.72752	-.03558
.76314	.04578	.77668	-.02466
.80756	.03761	.82348	-.01559
.84854	.03017	.86677	-.00859
.88537	.02335	.90545	-.00370
.91763	.01694	.93852	-.00075
.94523	.01101	.96509	.00054
.96799	.00600	.98446	.00065
.98528	.00245	.99612	.00024
.99623	.00054	1.00000	.00000
1.00000	.00000		

Table 2. Model Orifice Locations

Upper Surface			Lower Surface		
x/c	x, mm	y, mm	x/c	x, mm	y, mm
0.000	0.0	127.0	0.002	1.2	128.0
.002	1.2	200.0	.004	2.4	129.0
.004	2.4	199.0	.006	3.6	130.0
.006	3.6	198.0	.008	4.8	131.0
.008	4.8	197.0	.012	7.2	132.0
.012	7.2	196.0	.016	9.6	133.0
.016	9.6	195.0	.020	12.0	134.0
.020	12.0	194.0	.024	14.4	135.0
.024	14.4	193.0	.028	16.8	136.0
.028	16.8	192.0	.032	19.2	137.0
.032	19.2	191.0	.040	24.0	138.0
.040	24.0	190.0	.048	28.8	139.0
.048	28.8	189.0	.064	38.4	141.0
.064	38.4	187.0	.100	60.0	145.0
.100	60.0	183.0	.150	90.0	150.0
.150	90.0	178.0	.200	120.0	155.0
.200	120.0	173.0	.250	150.0	160.0
.250	150.0	168.0	.300	180.0	165.0
.300	180.0	163.0	.350	210.0	170.0
.350	210.0	158.0	.400	240.0	175.0
.400	240.0	153.0	.410	246.0	176.0
.450	270.0	148.0	.420	252.0	177.0
.460	276.0	147.0	.430	258.0	178.0
.470	282.0	146.0	.440	264.0	179.0
.480	288.0	145.0	.450	270.0	180.0
.490	294.0	144.0	.460	276.0	181.0
.500	300.0	143.0	.470	282.0	182.0
.510	306.0	142.0	.480	288.0	183.0
.520	312.0	141.0	.490	294.0	184.0
.530	318.0	140.0	.500	300.0	185.0
.540	324.0	139.0	.510	306.0	186.0

Table 2. Model Orifice Locations (Concluded)

Upper Surface			Lower Surface		
x/c	x, mm	y, mm	x/c	x, mm	y, mm
.550	330.0	138.0	.520	312.0	187.0
.560	336.0	137.0	.530	318.0	188.0
.570	342.0	136.0	.540	324.0	189.0
.580	348.0	135.0	.550	330.0	190.0
.590	354.0	134.0	.560	336.0	191.0
.600	360.0	133.0	.570	342.0	192.0
.610	366.0	132.0	.580	348.0	193.0
.620	372.0	131.0	.590	354.0	194.0
.630	378.0	130.0	.600	360.0	195.0
.640	384.0	129.0	.610	366.0	196.0
.650	390.0	128.0	.620	372.0	197.0
.700	420.0	133.0	.630	378.0	198.0
.750	450.0	138.0	.640	384.0	199.0
.800	480.0	143.0	.650	390.0	200.0
.850	510.0	148.0	.700	420.0	195.0
.880	528.0	151.0	.750	450.0	190.0
.900	540.0	153.0	.800	480.0	185.0
.920	552.0	155.0	.850	510.0	180.0
.940	564.0	157.0	.880	528.0	177.0
.960	576.0	159.0	.900	540.0	175.0
.980	588.0	161.0	.920	552.0	173.0
1.000	600.0	165.0	.940	564.0	171.0
			.960	576.0	169.0
			.980	588.0	167.0

c = 600.00 mm (23.622 in.)

Microsoft F

Table 3. Airfoil Design Specifications (S809)

Minimum lift coefficient	-
Maximum lift coefficient	1.0
«Design» lift coefficient	0.5
Lower limit of laminar bucket	0.2
Upper limit of laminar bucket	0.8
Zero-lift pitching-moment coefficient	$\geq -0.05$
Reynolds number	$2.0 \times 10^6$
Thickness	0.21c

Table 4. Roughness Size and Location

Reynolds Number	Upper Surface			Lower Surface		
	Grit Number	Nominal Size, mm/in.	x/c	Grit Number	Nominal Size, mm/in.	x/c
$1.0 \times 10^6$	80	0.211/0.0083	0.02	46	0.419/0.0165	0.05
$1.5 \times 10^6$	120	.124/.0049	.02	70	.249/.0098	.05
$2.0 \times 10^6$	120	.124/.0049	.02	70	.249/.0098	.05
$2.5 \times 10^6$	120	.124/.0049	.02	70	.249/.0098	.05
$3.0 \times 10^6$	120	.124/.0049	.02	70	.249/.0098	.05

Table 5. AOA1 > Geometry

Object Name	Geometry
State	Fully Defined
<b>Definition</b>	
Source	C:\Users\User\Desktop\2D simulation Fluent\2D Fluent_files\dp0\Geom-2\DM\Geom-2.agdb
Type	DesignModeler
Length Unit	Meters
<b>Bounding Box</b>	
Length X	21.721 m
Length Y	14. m
Length Z	0. m
<b>Properties</b>	
Volume	0. m <sup>3</sup>
Scale Factor Value	1.
<b>Statistics</b>	
Bodies	4
Active Bodies	4
Nodes	157895
Elements	157585
Mesh Metric	None
<b>Basic Geometry Options</b>	

Solid Bodies	Yes
Surface Bodies	Yes
Line Bodies	Yes
Parameters	Independent
Parameter Key	
Attributes	Yes
Attribute Key	
Named Selections	Yes
Named Selection Key	
Material Properties	Yes
<b>Advanced Geometry Options</b>	
Use Associativity	Yes
Coordinate Systems	Yes
Coordinate System Key	
Reader Mode Saves Updated File	No
Use Instances	Yes
Smart CAD Update	Yes
Compare Parts On Update	No
Attach File Via Temp File	Yes
Temporary Directory	C:\Users\User\AppData\Local\Temp
Analysis Type	3-D
Mixed Import Resolution	None
Decompose Disjoint Geometry	Yes
Enclosure and Symmetry Processing	Yes

Table 6. AOA1 > Geometry > Parts

Object Name	Line Body	Surface Body	Surface Body	Surface Body
State	Hidden	Meshed	Fully Defined	
<b>Graphics Properties</b>				
Visible	No	Yes		
Transparency			1	
<b>Definition</b>				
Suppressed	No			
Coordinate System	Default Coordinate System			
Offset Mode	Refresh on Update			
Offset Type	Centroid	Middle		
Model Type	Beam			
Reference Frame	Lagrangian			
Thickness	0. m			
Thickness Mode	Refresh on Update			
Behavior	None			
Body of Influence			Yes	
<b>Material</b>				
Fluid/Solid	Defined By Geometry (Solid)			
<b>Bounding Box</b>				
Length X	1.0101 m	21. m		
Length Y	0.12421 m	14. m		
Length Z	0. m			
<b>Properties</b>				
Volume	0. m <sup>3</sup>			
Length	2.0679 m			
Cross Section	0			

Cross Section Area		
Cross Section IYY		
Cross Section IZZ		
Centroid X		4.5988 m
Centroid Y		4.0005e-002 m
Centroid Z		0. m
Surface Area(approx.)		272.89 m <sup>2</sup>
<b>Statistics</b>		
Nodes	90	157805
Elements	45	157540
Mesh Metric	None	
<b>CAD Attributes</b>		
DMSheetThickness		0

Table 7. AOA1 > Connections

Object Name	Connections
State	Fully Defined
<b>Auto Detection</b>	
Generate Automatic Connection On Refresh	Yes
<b>Transparency</b>	
Enabled	Yes

Table 8. AOA1 > Mesh

Object Name	Mesh
State	Solved
<b>Display</b>	
Display Style	Body Color
<b>Defaults</b>	
Physics Preference	CFD
Solver Preference	Fluent
Relevance	0
Export Format	Standard
Shape Checking	CFD
Element Midside Nodes	Dropped
<b>Sizing</b>	
Size Function	Proximity and Curvature
Use Uniform Size Function For Sheets	No
Relevance Center	Fine
Initial Size Seed	Active Assembly
Smoothing	High
Span Angle Center	Fine
Curvature Normal Angle	Default (18.0 °)
Num Cells Across Gap	Default (3)
Proximity Size Function Sources	Faces and Edges
Min Size	Default (3.7725e-003 m)
Proximity Min Size	Default (3.7725e-003 m)
Max Face Size	0.10 m
Max Tet Size	0.10 m
Growth Rate	Default (1.20 )
Automatic Mesh Based Defeaturing	On
Defeaturing Tolerance	Default (1.8863e-003 m)
Minimum Edge Length	4.906e-003 m
<b>Inflation</b>	
Use Automatic Inflation	None

Inflation Option	Smooth Transition
Transition Ratio	0.272
Maximum Layers	2
Growth Rate	1.2
Inflation Algorithm	Pre
View Advanced Options	No
<b>Assembly Meshing</b>	
Method	None
<b>Advanced</b>	
Number of CPUs for Parallel Part Meshing	Program Controlled
Straight Sided Elements	
Number of Retries	0
Rigid Body Behavior	Dimensionally Reduced
Mesh Morphing	Disabled
Triangle Surface Mesher	Program Controlled
Topology Checking	No
Use Sheet Thickness for Pinch	No
Pinch Tolerance	Default (3.3953e-003 m)
Generate Pinch on Refresh	No
Sheet Loop Removal	No
<b>Statistics</b>	
Nodes	157895
Elements	157585
Mesh Metric	None

Table 9. AOA1 > Mesh > Mesh Controls

Object Name	<i>Body Sizing</i>	<i>Edge Sizing</i>	<i>Edge Sizing 2</i>	<i>Inflation</i>
State	Fully Defined			
<b>Scope</b>				
Scoping Method	Geometry Selection			
Geometry	1 Body	2 Edges		1 Face
<b>Definition</b>				
Suppressed	No			
Type	Body of Influence	Number of Divisions		
Bodies of Influence	2 Bodies			
Element Size	2.e-002 m			
Growth Rate	1.20			1.2
Local Min Size	Default (3.7725e-003 m)			
Number of Divisions		250	5	
Behavior	Hard			
Bias Type	No Bias			
Boundary Scoping Method				Geometry Selection
Boundary				4 Edges
Inflation Option				First Layer Thickness
First Layer Height				1.e-006 m
Maximum Layers				100
Inflation Algorithm				Pre

Table 10. AOA3 > Geometry

Object Name	<i>Geometry</i>
State	Fully Defined
<b>Definition</b>	
Source	C:\Users\User\Desktop\2D simulation Fluent\2D Fluent_files\dp0\Geom-

	3DMGeom-3.agdb
Type	DesignModeler
Length Unit	Meters
<b>Bounding Box</b>	
Length X	21.721 m
Length Y	14. m
Length Z	0. m
<b>Properties</b>	
Volume	0. m <sup>3</sup>
Scale Factor Value	1.
<b>Statistics</b>	
Bodies	4
Active Bodies	4
Nodes	133542
Elements	133197
Mesh Metric	None
<b>Basic Geometry Options</b>	
Solid Bodies	Yes
Surface Bodies	Yes
Line Bodies	Yes
Parameters	Independent
Parameter Key	
Attributes	Yes
Attribute Key	
Named Selections	Yes
Named Selection Key	
Material Properties	Yes
<b>Advanced Geometry Options</b>	
Use Associativity	Yes
Coordinate Systems	Yes
Coordinate System Key	
Reader Mode Saves Updated File	No
Use Instances	Yes
Smart CAD Update	Yes
Compare Parts On Update	No
Attach File Via Temp File	Yes
Temporary Directory	C:\Users\User\AppData\Local\Temp
Analysis Type	3-D
Mixed Import Resolution	None
Decompose Disjoint Geometry	Yes
Enclosure and Symmetry Processing	Yes

Table 11. AOA3 > Geometry > Parts

Object Name	Line Body	Surface Body	Surface Body	Surface Body
State	Hidden	Meshed	Fully Defined	
<b>Graphics Properties</b>				
Visible	No	Yes		
Transparency				1
<b>Definition</b>				
Suppressed	No			
Coordinate System	Default Coordinate System			
Offset Mode	Refresh on Update			

Offset Type	Centroid	Middle	
Model Type	Beam		
Reference Frame	Lagrangian		
Thickness		0. m	
Thickness Mode		Refresh on Update	
Behavior			None
Body of Influence			Yes
<b>Material</b>			
Fluid/Solid	Defined By Geometry (Solid)		
<b>Bounding Box</b>			
Length X	1.0087 m	21. m	
Length Y	0.13615 m	14. m	
Length Z	0. m		
<b>Properties</b>			
Volume	0. m <sup>3</sup>		
Length	2.0679 m		
Cross Section	0		
Cross Section Area			
Cross Section IYY			
Cross Section IZZ			
Centroid X		4.5988 m	
Centroid Y		4.0009e-002 m	
Centroid Z		0. m	
Surface Area(approx.)		272.89 m <sup>2</sup>	
<b>Statistics</b>			
Nodes	88	133454	
Elements	44	133153	
Mesh Metric	None		
<b>CAD Attributes</b>			
DMSheetThickness			0

Table 12. AOA3 > Connections

Object Name	Connections
State	Fully Defined
<b>Auto Detection</b>	
Generate Automatic Connection On Refresh	Yes
<b>Transparency</b>	
Enabled	Yes

Table 13. AOA3 > Mesh

Object Name	Mesh
State	Solved
<b>Display</b>	
Display Style	Body Color
<b>Defaults</b>	
Physics Preference	CFD
Solver Preference	Fluent
Relevance	0
Export Format	Standard
Shape Checking	CFD
Element Midside Nodes	Dropped
<b>Sizing</b>	
Size Function	Proximity and Curvature
Use Uniform Size Function For Sheets	No

Relevance Center	Fine
Initial Size Seed	Active Assembly
Smoothing	High
Span Angle Center	Fine
Curvature Normal Angle	Default (18.0 °)
Num Cells Across Gap	Default (3)
Proximity Size Function Sources	Faces and Edges
Min Size	Default (3.7725e-003 m)
Proximity Min Size	Default (3.7725e-003 m)
Max Face Size	0.10 m
Max Tet Size	0.10 m
Growth Rate	Default (1.20 )
Automatic Mesh Based Defeaturing	On
Defeaturing Tolerance	Default (1.8863e-003 m)
Minimum Edge Length	4.906e-003 m
<b>Inflation</b>	
Use Automatic Inflation	None
Inflation Option	Smooth Transition
Transition Ratio	0.272
Maximum Layers	2
Growth Rate	1.2
Inflation Algorithm	Pre
View Advanced Options	No
<b>Assembly Meshing</b>	
Method	None
<b>Advanced</b>	
Number of CPUs for Parallel Part Meshing	Program Controlled
Straight Sided Elements	
Number of Retries	0
Rigid Body Behavior	Dimensionally Reduced
Mesh Morphing	Disabled
Triangle Surface Mesher	Program Controlled
Topology Checking	No
Use Sheet Thickness for Pinch	No
Pinch Tolerance	Default (3.3953e-003 m)
Generate Pinch on Refresh	No
Sheet Loop Removal	No
<b>Statistics</b>	
Nodes	133542
Elements	133197
Mesh Metric	None

Table 14. AOA3 > Mesh > Mesh Controls

Object Name	<i>Body Sizing</i>	<i>Edge Sizing</i>	<i>Edge Sizing 2</i>	<i>Inflation</i>
State	Fully Defined			
<b>Scope</b>				
Scoping Method	Geometry Selection			
Geometry	1 Body	2 Edges		1 Face
<b>Definition</b>				
Suppressed	No			
Type	Body of Influence	Number of Divisions		
Bodies of Influence	2 Bodies			
Element Size	2.e-002 m			
Growth Rate	1.20			1.2

Local Min Size	Default (3.7725e-003 m)		
Number of Divisions	250	5	
Behavior	Hard		
Bias Type	No Bias		
Boundary Scoping Method			Geometry Selection
Boundary			4 Edges
Inflation Option			Total Thickness
Number of Layers			50
Maximum Thickness			1.e-002 m
Inflation Algorithm			Pre

Table 15. AOA5 > Geometry

Object Name	Geometry
State	Fully Defined
<b>Definition</b>	
Source	C:\Users\User\Desktop\2D simulation Fluent\2D Fluent_files\dp0\Geom-1\DM\Geom-1.agdb
Type	DesignModeler
Length Unit	Meters
<b>Bounding Box</b>	
Length X	21.721 m
Length Y	14. m
Length Z	0. m
<b>Properties</b>	
Volume	0. m <sup>3</sup>
Scale Factor Value	1.
<b>Statistics</b>	
Bodies	4
Active Bodies	4
Nodes	137495
Elements	137141
Mesh Metric	None
<b>Basic Geometry Options</b>	
Solid Bodies	Yes
Surface Bodies	Yes
Line Bodies	Yes
Parameters	Independent
Parameter Key	
Attributes	Yes
Attribute Key	
Named Selections	Yes
Named Selection Key	
Material Properties	Yes
<b>Advanced Geometry Options</b>	
Use Associativity	Yes
Coordinate Systems	Yes
Coordinate System Key	
Reader Mode Saves Updated File	No
Use Instances	Yes
Smart CAD Update	Yes
Compare Parts On Update	No
Attach File Via Temp File	Yes
Temporary Directory	C:\Users\User\AppData\Local\Temp

Analysis Type	3-D
Mixed Import Resolution	None
Decompose Disjoint Geometry	Yes
Enclosure and Symmetry Processing	Yes

Table 16. AOA5 > Geometry > Parts

Object Name	Line Body	Surface Body	Surface Body	Surface Body
State	Meshed		Fully Defined	
<b>Graphics Properties</b>				
Visible	Yes			
Transparency	1			
<b>Definition</b>				
Suppressed	No			
Coordinate System	Default Coordinate System			
Offset Mode	Refresh on Update			
Offset Type	Centroid	Middle		
Model Type	Beam			
Reference Frame	Lagrangian			
Thickness	0. m			
Thickness Mode	Refresh on Update			
Behavior	None			
Body of Influence	Yes			
<b>Material</b>				
Fluid/Solid	Defined By Geometry (Solid)			
<b>Bounding Box</b>				
Length X	1.0061 m	21. m		
Length Y	0.1615 m	14. m		
Length Z	0. m			
<b>Properties</b>				
Volume	0. m <sup>3</sup>			
Length	2.0679 m			
Cross Section	0			
Cross Section Area				
Cross Section IYY				
Cross Section IZZ				
Centroid X	4.5988 m			
Centroid Y	4.0013e-002 m			
Centroid Z	0. m			
Surface Area(approx.)	272.89 m <sup>2</sup>			
<b>Statistics</b>				
Nodes	166	137329		
Elements	83	137058		
Mesh Metric	None			
<b>CAD Attributes</b>				
DMSheetThickness	0			

Table 17. AOA5 > Connections

Object Name	Connections
State	Fully Defined
<b>Auto Detection</b>	
Generate Automatic Connection On Refresh	Yes
<b>Transparency</b>	

Enabled	Yes
---------	-----

Table 18. AOA5 > Mesh

Object Name	Mesh
State	Solved
<b>Display</b>	
Display Style	Body Color
<b>Defaults</b>	
Physics Preference	CFD
Solver Preference	Fluent
Relevance	0
Export Format	Standard
Shape Checking	CFD
Element Midside Nodes	Dropped
<b>Sizing</b>	
Size Function	Proximity and Curvature
Use Uniform Size Function For Sheets	No
Relevance Center	Fine
Initial Size Seed	Active Assembly
Smoothing	High
Span Angle Center	Fine
Curvature Normal Angle	Default (18.0 °)
Num Cells Across Gap	Default (3)
Proximity Size Function Sources	Faces and Edges
Min Size	Default (3.7725e-003 m)
Proximity Min Size	Default (3.7725e-003 m)
Max Face Size	0.10 m
Max Tet Size	0.10 m
Growth Rate	Default (1.20 )
Automatic Mesh Based Defeaturing	On
Defeaturing Tolerance	Default (1.8863e-003 m)
Minimum Edge Length	4.906e-003 m
<b>Inflation</b>	
Use Automatic Inflation	None
Inflation Option	Smooth Transition
Transition Ratio	0.272
Maximum Layers	2
Growth Rate	1.2
Inflation Algorithm	Pre
View Advanced Options	No
<b>Assembly Meshing</b>	
Method	None
<b>Advanced</b>	
Number of CPUs for Parallel Part Meshing	Program Controlled
Straight Sided Elements	
Number of Retries	0
Rigid Body Behavior	Dimensionally Reduced
Mesh Morphing	Disabled
Triangle Surface Mesher	Program Controlled
Topology Checking	No
Use Sheet Thickness for Pinch	No
Pinch Tolerance	Default (3.3953e-003 m)
Generate Pinch on Refresh	No
Sheet Loop Removal	No

Statistics	
Nodes	137495
Elements	137141
Mesh Metric	None

Table 19. AOA5 > Mesh > Mesh Controls

Object Name	Body Sizing	Inflation	Edge Sizing	Edge Sizing 2
State	Fully Defined			
Scope				
Scoping Method	Geometry Selection			
Geometry	1 Body	1 Face	2 Edges	1 Edge
Definition				
Suppressed	No			
Type	Body of Influence		Number of Divisions	
Bodies of Influence	2 Bodies			
Element Size	2.e-002 m			
Growth Rate	1.20	1.2		
Local Min Size	Default (3.7725e-003 m)			
Boundary Scoping Method		Geometry Selection		
Boundary		4 Edges		
Inflation Option		Total Thickness		
Number of Layers		50		
Maximum Thickness		1.e-002 m		
Inflation Algorithm		Pre		
Number of Divisions			250	5
Behavior			Hard	
Bias Type			No Bias	

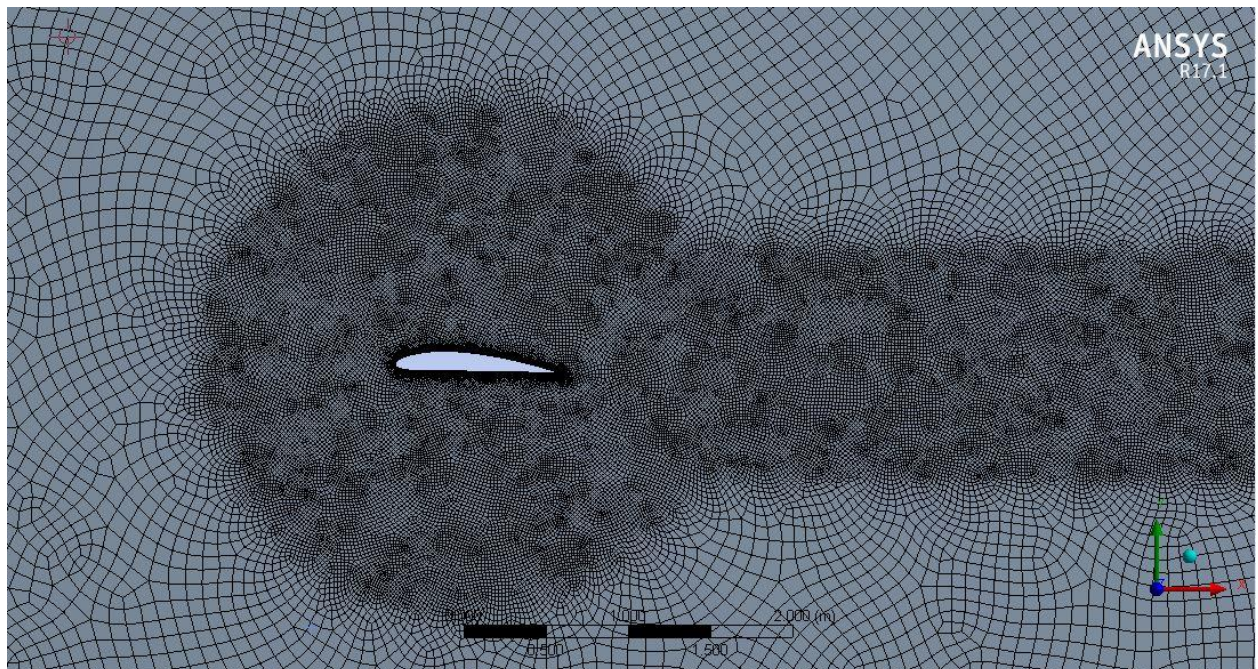


Figure 1. Scaled mesh of an airfoil at an angle of 1°

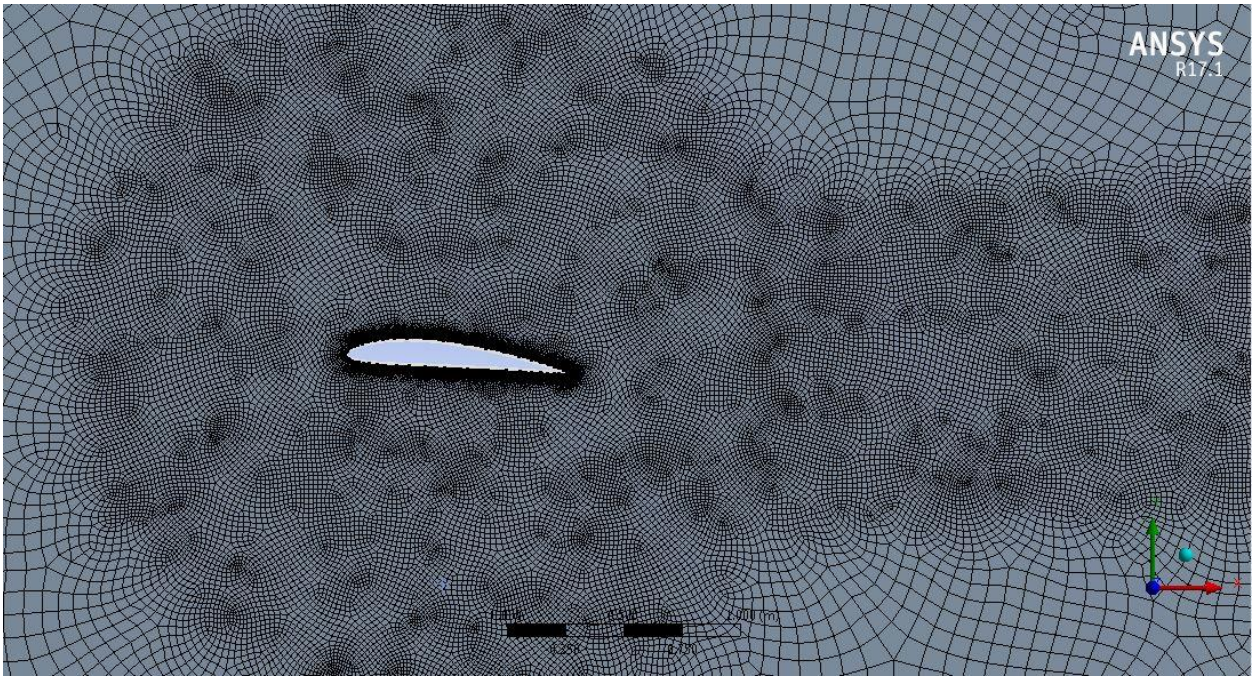


Figure 2. Scaled mesh of an airfoil at an angle of  $3^\circ$

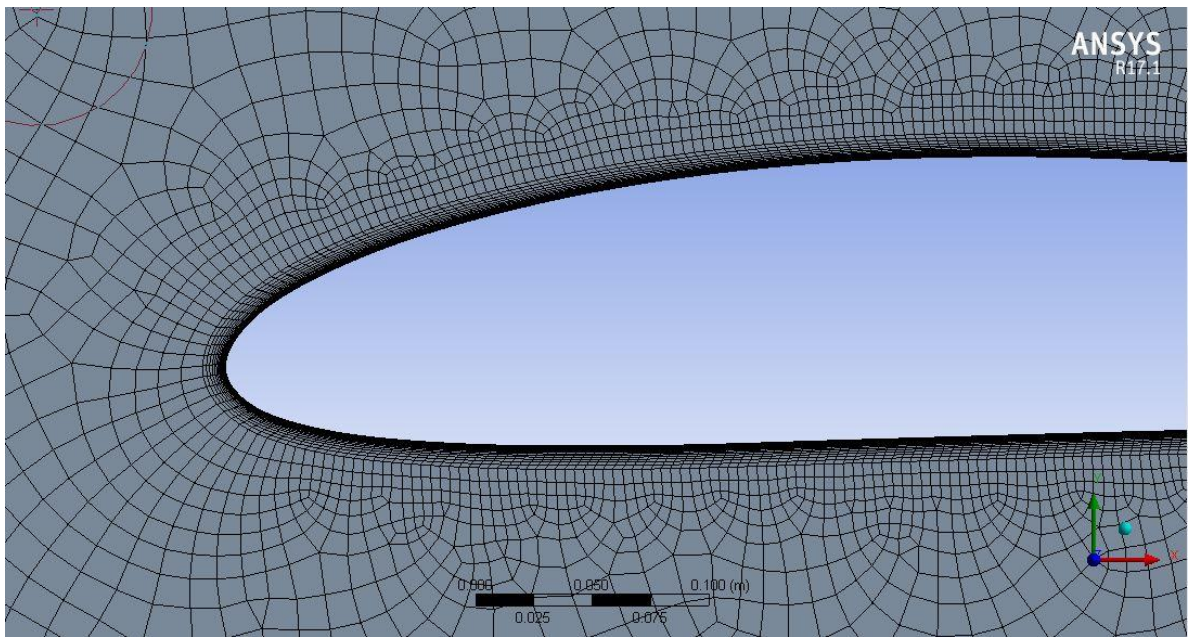


Figure 3. Inflation of an airfoil mesh at an angle of  $1^\circ$

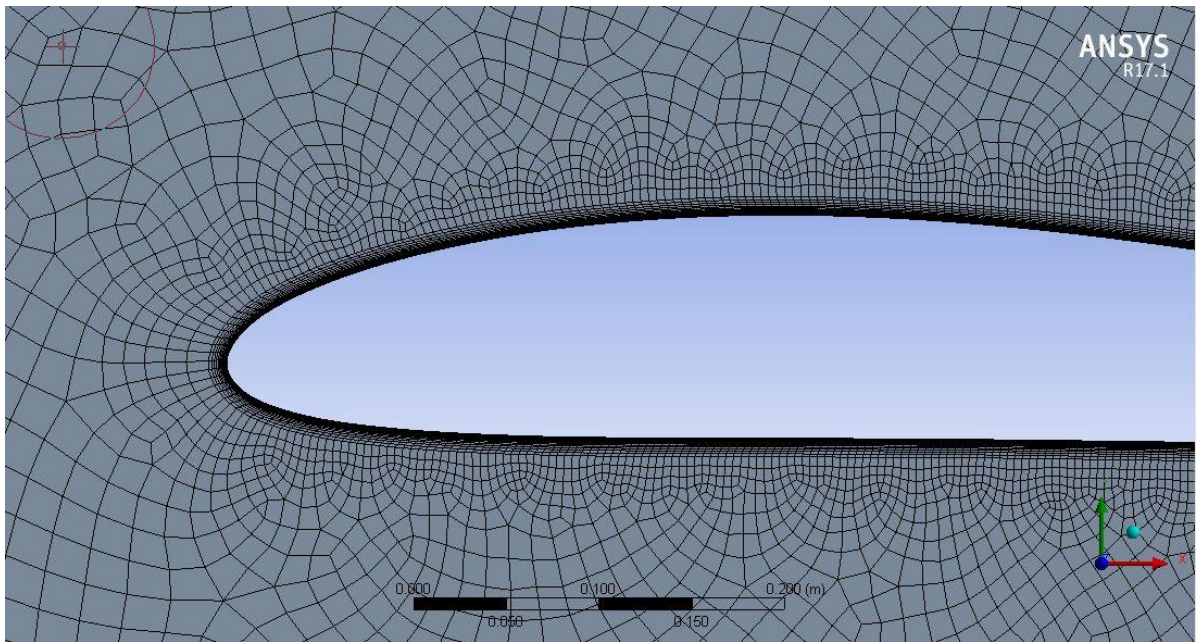


Figure 4. Inflation of an airfoil mesh at an angle of  $3^\circ$

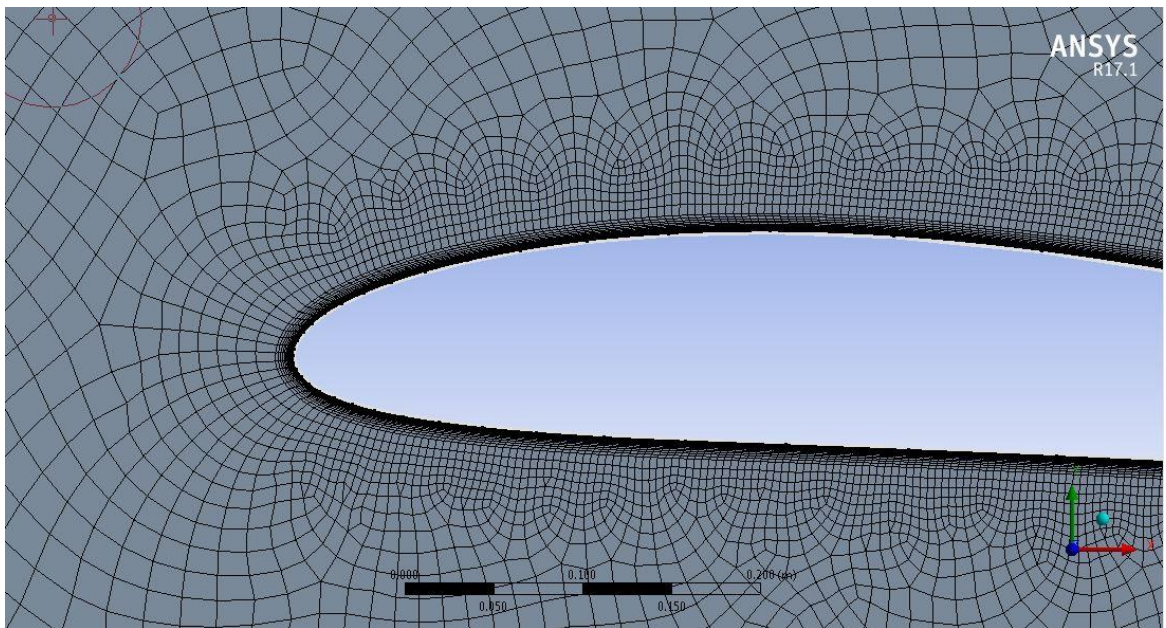


Figure 5. Inflation of an airfoil mesh at an angle of  $5^\circ$